3-2001

Investigation of Gravity Waves via the Rotational Temperature of Hydroxyl Nightglow

Erin C. Willingham

INVESTIGATION OF GRAVITY WAVES VIA THE ROTATIONAL TEMPERATURE OF HYDROXYL NIGHTGLOW

THESIS

Erin C.W. Willingham, Captain, USAF

AFIT/GM/ENP/01M-09

DEPARTMENT OF THE AIR FORCE
AIR UNIVERSITY

AIR FORCE INSTITUTE OF TECHNOLOGY

Wright-Patterson Air Force Base, Ohio

AFIT/GM/ENP/01M-09

INVESTIGATION OF GRAVITY WAVES VIA THE ROTATIONAL TEMPERATURE OF HYDROXYL NIGHTGLOW

THESIS

Erin C.W. Willingham, Captain, USAF

AFIT/GM/ENP/01M-09

The views expressed in this thesis are those of the author and do not reflect the official policy or position of the Department of Defense or the U.S. Government.

AFIT/GM/ENP/01M-09

INVESTIGATION OF GRAVITY WAVES VIA THE ROTATIONAL TEMPERATURE OF HYDROXYL NIGHTGLOW

THESIS

Presented to the Faculty of the Graduate School of Engineering

of the Air Force Institute of Technology

Air University

Air Education and Training Command

In Partial Fulfillment of the Requirements for the

Degree of Master of Science

Erin C.W. Willingham, B.S.,

Captain, USAF

March 2001

AFIT/GM/ENP/01M-09

INVESTIGATION OF GRAVITY WAVES VIA THE ROTATIONAL TEMPERATURE OF HYDROXYL NIGHTGLOW

Erin C.W. Willingham, B.S.,
Captain, USAF

Approved:

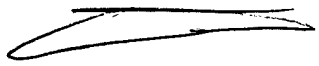

2 MAR 01

Lt Col Glen P. Perram
Chairman, Advisory Committee

date

2 MAR 01

Lt Col Michael K. Walters
Member, Advisory Committee

date

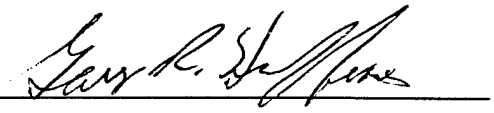

2 March 2001

Maj Gary R. Huffines
Member, Advisory Committee

date

Acknowledgments

The shear magnitude of knowledge necessary to complete this research has required me to seek assistance from many individuals to whom I owe a great deal of thanks. First, I would like to express my sincere gratitude to my advisors, Lt Col Glen Perram, Lt Col Mike Walters, and Maj Gary Huffines for their confidence in my ability to bring this enormous task to completion and for giving me a great deal of latitude in the scope of this project.

Next, I owe many thanks to Greg Smith, AFIT/ENP laboratory technician, for his advice, assistance, and friendship. His support and expertise was greatly needed and appreciated.

I thank Dr. David Weeks for his insight on telescope instrumentation and astrophotography.

Lastly, I thank my wife, for her patience and understanding during the long hours spent completing this project.

Erin C.W. Willingham

Table of Contents

List of Figures

List of Tables

Abstract

Measurement of the vibration and rotation bands of mesospheric hydroxyl radicals (OH) has been conducted during the past two decades using ground-based and space-based interferometers to take temperature and wind measurements from 70-100 km in altitude. Gravity waves that pass through the mesosphere can be measured by determining the variance over time of the rotational temperature of the OH emissions. Several attempts were made to take spectrum measurements of the nightglow from hydroxyl radicals in the mesosphere using a custom hardware configuration that included a telescope and grating monochrometer optimized for the visible and near infrared. Quantifying gravity wave activity was the ultimate objective of this experiment. No spectrum of OH nightglow was recorded. The instrumentation was not sensitive enough to pick up the weak signal. This thesis is primarily a characterization of the equipment, its capabilities, and its limitations.

INVESTIGATION OF GRAVITY WAVES VIA THE ROTATIONAL TEMPERATURE OF HYDROXYL NIGHTGLOW

I. Introduction

1.1 Motivation

Observations of gravity waves in the near infrared and visible wavelength nightglow emissions (altitude of ~80-100 km) have been reported by a number of researchers over the past two decades. Most measurements have been made through the use of Michelson interferometers that were either ground-based or space-based on satellites or space shuttles. Due to the expense of the systems, measurements are made infrequently and at few locations.

If gravity waves could be measured continuously at several locations across the United States, then the resulting data could be studied on a synoptic scale, which has never been done before. The advantages are obvious. A better understanding of atmospheric processes is certain; improvements in weather forecast products are possible. For this to become a reality in the future, numerous ground-based instruments would need to be in place throughout the United States. The instrumentation would need to be relatively inexpensive.

This research was an attempt to measure gravity waves using a simple grating monochrometer optimized for the visible and near infrared range, with a large telescope used to channel nighttime radiation into the monochrometer.

1.2 Problem and Objective

The atmosphere is a large fluid mass with waves traveling throughout. Some waves are created by jet streams and smaller air currents passing over rough terrain. All large-scale weather-producing systems such as hurricanes, mesoscale convective complexes, and supercell systems create strong waves that can travel around the globe. In fact, any density discontinuity within the atmosphere can create a wave. The restoring force for these waves is buoyancy (or a combination of buoyancy with the Coriolis "force"). Since buoyancy in the atmosphere is a result of gravity, these waves are known as gravity waves.

Atmospheric gravity waves were discovered first as mathematical solutions to physical formulae, and later observed in nature. Sometimes they can even be observed by the naked eye. When wind shear is very strong over a mountain, the gravity wave that can result (known as a Kelvin-Helmholtz instability wave) may have clouds form in their wake showing a wavelike structure. However, the vast majority of gravity waves are not seen with unaided eyes. It is difficult to measure what cannot be seen. However, if they could be measured then they might be useful in weather forecasting.

The ultimate objective of this research was to obtain quantitative measurements of gravity waves activity. Using a custom hardware configuration that included a telescope connected to a monochrometer, radiation emissions from the night sky (known as nightglow) were to be focused into the monochrometer by the telescope resulting in a radiation spectrum from the night sky. One of the strongest emissions from the night sky is from a layer of hydroxyl (OH) molecules 86 km above ground level. As gravity waves pass through this layer of OH, the waves impart energy to the molecules. These excited

molecules will then radiate this additional energy into the atmosphere as they return to equilibrium. There will be a change in the rotational temperature of the OH, which will be measured by taking several spectra over time. Temperature variations over time are observed. It is this temperature variance that is a possible indication of gravity wave activity.

A secondary objective was to determine any cyclical or diurnal trends in the gravity wave activity. Specifically, with a large supercell thunderstorm or mesoscale convective complex within an arbitrary distance, is there an appreciable increase in rotational temperature variance. This could possibly indicate that some of the gravity wave activity in the mesosphere originated from the storm.

1.3 Research Importance

In the future, gravity wave measurements may be available as data input for the improvement of weather analysis products. If gravity wave activity can be measured by relatively inexpensive ground-based spectrometers, then a "sensor" could be at any weather observing station. The data stream of continuous measurements from these sensors would be sent to weather data processing centers as input data for a variety of analysis products. Hopefully the addition of this new type of input data would improve the forecast accuracy of the products.

Of additional importance is the forecasting of turbulence. Severe turbulence is hazardous to aircraft. Also, moderate to severe thunderstorms generate gravity waves. These waves can then trigger the creation of additional thunderstorms, strengthen existing thunderstorms, and deliver turbulent conditions over great distances.

1.4 Summary of Results

The collection of nightglow spectra was unfruitful. No spectra of OH were recorded; no gravity wave activity was measured. When attempting to measure all nightglow radiation, some was received, as shown on figure 18. A filter, which only allows only the 762 nm wavelength from passing through, was used to demonstrate if any discovered signal is O_2 or OH. The strongest nightglow intensity is from O_2 and OH at a wavelength of 762 nm (Bellaire: 1997). If an intensity spike is found without using the filter, than that wavelength interval is then scanned a second time while using the filter. If the intensity spike is absent while using the filter, then what was measured was not O_2 or OH. From the research done,

When searching all of the visible and near infrared spectrum for contributors to the total radiation received, a weak intensity was found at 773 nm. This is shown in figures 19 and 20. Use of the filter indicated that the intensity spike was not O_2 or OH; the intensity's origin is unknown.

1.5 Thesis Organization

In this chapter, the motivation for this research was presented, followed by the problems to be addressed in this document, the importance of this research, and a summary of the results. Chapter 2 will give background into the knowledge of spectroscopy, gravity waves, and atmospheric hydroxyl needed to perform this experiment. In addition, relevant previous studies are reviewed. The hardware is described in chapter 3, including configuration, calibration, and limitations. This is followed by the methodology, in chapter 4. Chapter 5 discusses the analysis and results.

Lastly, Chapter 6 will provide the conclusions and recommendations resulting from this research, and ideas for future research topics. The appendix is a collection of photos of all the instrumentation used in the experiments. These photos were separated from the body text to allow for easier reading.

II. Subject Background

2.1 Overview

This chapter reviews the subject background necessary to appreciate the experimental research carried out in this thesis. The chapter gives brief overviews of spectroscopy, gravity waves, and the layer of OH in the mesosphere. Lastly, previous studies in this area of research that have relevance to the current project will be discussed.

2.2 Spectroscopy Background

Spectroscopy is the study of the exchange of energy between radiation and matter. Electromagnetic radiation is a transverse waveform; it consists of oscillating electric and magnetic fields that point transversely to the direction of propagation of the wave. Figure 1 is a diagram of an electromagnetic wave. Light is an electromagnetic wave that can be represented by the plane wave

$$\mathbf{E}(\mathbf{r},t) = \mathbf{E}_o\cos(\mathbf{k}\bullet\mathbf{r}-\omega t+\phi_o). \qquad (1)$$

where **E** is the electric field perpendicular to, and propagating in, a vector direction **k**. **E** travels in the direction of vector **r** and has an angular frequency $\omega = 2\pi f$, where f is frequency in hertz. ϕ_o is an initial phase angle, and t is time (Bernath: 1995).

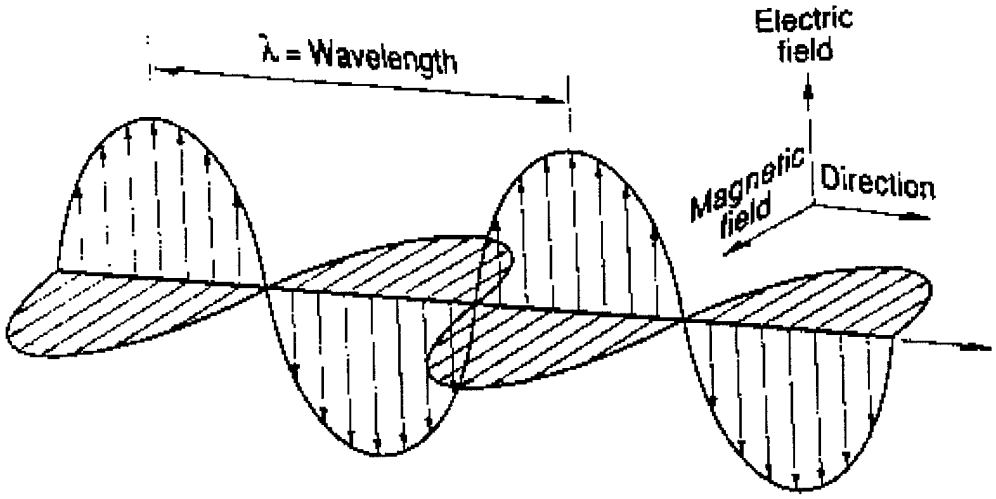

Figure 1. Diagram of an electromagnetic wave. All bodies that have a temperature higher than absolute zero (0° Kelvin) radiate electromagnetic energy of varying wavelengths. Electromagnetic energy passes through space at the speed of light in the form of sinusoidal waves. The wavelength is the distance from wavecrest to wavecrest. (Brown: 1998)

A spectrum is the variation of the signal intensity as the frequency of a given radiation is scanned. It is a distribution of energy often represented graphically as an interval of wave measurement such as wavenumber, wavelength, or frequency (X-axis) compared to intensity (Y-axis). Figure 2 is an example. A spectrum of a molecule contains many emission (or absorption) features called lines organized into a band associated with a particular mode of vibration.

When a molecule is excited in an electrical discharge a regular series of emission lines is observed. In the 1850's Kirchoff and Bunsen established that each atom had a characteristic spectral signature (Bernath: 1995). In fact, the power of spectroscopy is the ability to identify specific atoms and molecules remotely because their spectra are all

different and uniquely characteristic. The energy from the atoms and molecules is transferred from the source to a detector in the form of electromagnetic radiation.

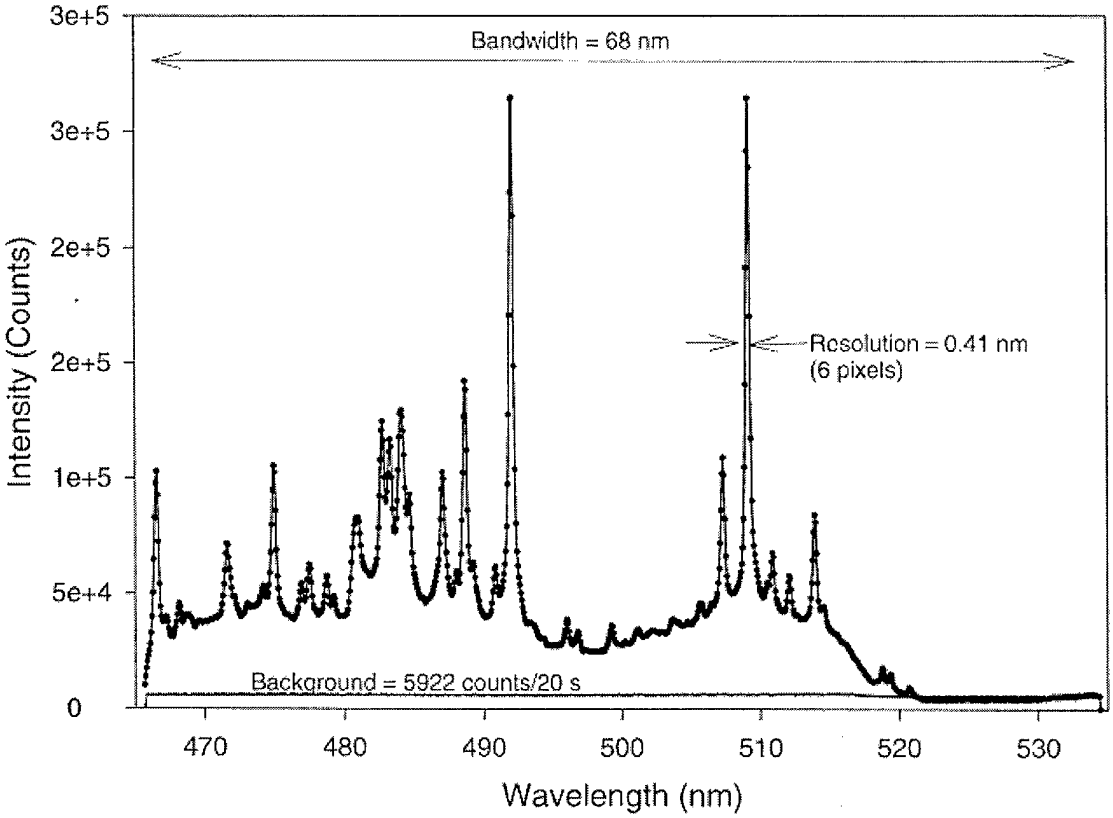

Figure 2. Emission spectrum of a plume. Spectrum interval is from 466 nm to 534nm showing relative intensity. This spectrum was taken by the author from a plume produced by laser ablation of a target consisting of yttrium, barium, and copper. Monochrometer incoming slit width was 20 μm with a period of integration of 20 s. The equipment configuration used is described in chapter 3, while chapter 5 discusses the results of the measurements.

If a light wave does not interact at all with the sample in a given frequency range, then the spectrum is flat and uninformative. However, if the radiation interacts at particular wavelengths, then energy is absorbed and various peaks occur in the spectrum. This corresponds to a reduction in intensity at the detector.

To develop graphs of OH rotational temperature, the relative intensity of OH emission lines over time is needed. Therefore, a discussion of intensity is in order. If the electric and magnetic field strengths are E and H, respectively, then energy density ρ is

$$\rho = \tfrac{1}{2}\,\varepsilon_o E^2 + \tfrac{1}{2}\,\mu_o H^2 \qquad (2)$$

where ε_o is the permittivity, μ_o is the permeability of a vacuum, and ρ is in $W/(J\ m^{-3})$. The energy is stored equally in the electric and magnetic fields. The intensity I of this light wave is the energy crossing a unit area per second ($J\ m^{-2}\ s^{-1}$)

$$I = \tfrac{1}{2}\,\varepsilon_o c E_o^{\,2} = \tfrac{1}{2}\,\mu_o c H_o^{\,2} \qquad (3)$$

where E_o and H_o are the amplitudes of the electric and magnetic sinusoidal waveforms, at their maximum fields (Brown: 1998).

In addition to considering light as a wave, it is sometimes necessary to describe light as a stream of particles called photons. Each photon carries an amount of energy *h*f, where *h* is Planck's constant and f is the frequency. Photons have no mass, yet they have linear momentum *h*f/c and angular momentum $\pm h/2\pi$ (Bernath: 1995).

How energy is exchanged between radiation and matter is fascinating. It involves the interaction between the oscillating electric field in the radiation with the appropriate dipole moment in the molecule. (Dipole moment being the product of either charge in an electric dipole with the distance separating them.) In order for this interaction to occur, the dipole moment must be oscillating in some way at the same frequency as the radiation field. Oscillations can be a result of rotation or vibration of the molecule. Matter can only respond to light at particular frequencies. Atoms and molecules only increase or decrease in energy amounts that correspond to discrete stationary states. The discrete

stationary amounts of energy is popularly known as the quantization of energy (Bernath: 1995). Molecules move only with certain amounts of energy. The exchange of energy corresponds to the photon giving up its energy hf to the molecule to raise it from a lower energy level E_1 to a higher one E_2. Therefore, conservation of energy requires

$$hf = E_2 - E_1. \tag{4}$$

(Brown: 1998). The molecule falls to a lower level and emits a photon of an appropriate frequency when energy is emitted in the form of light. The formula above states in symbols that the energy change produced in a molecule is proportional to the frequency of the radiation.

To absorb or emit radiation, molecules must move to different energy levels in one of three ways: induced absorption, induced emission, or spontaneous emission, as displayed in figure 3. Induced absorption results from the presence of a radiation amount of the precise frequency needed to drive a transition from the ground state to the excited state. Similarly, if the system is already in an excited state, then the addition of one or more photons of energy $h\nu$ can induce the system to make the transition to the ground state, i.e. the induced emission. Also, the system in the excited state can spontaneously emit a photon. In this research, the hydroxyl radicals are spontaneously emitting the energy they absorb from the passing gravity waves.

The energy change involved in spectroscopic transitions is measured in relative units of frequency or wavenumber. Wavenumber is defined as the inverse wavelength, usually cm^{-1}. Wavenumber is defined by

$$\varpi = 1/\lambda_{vac} = 1/(\lambda_{air}\eta_{air}). \tag{5}$$

This last formula is important since spectroscopy measurements are often made with their optical path through the air.

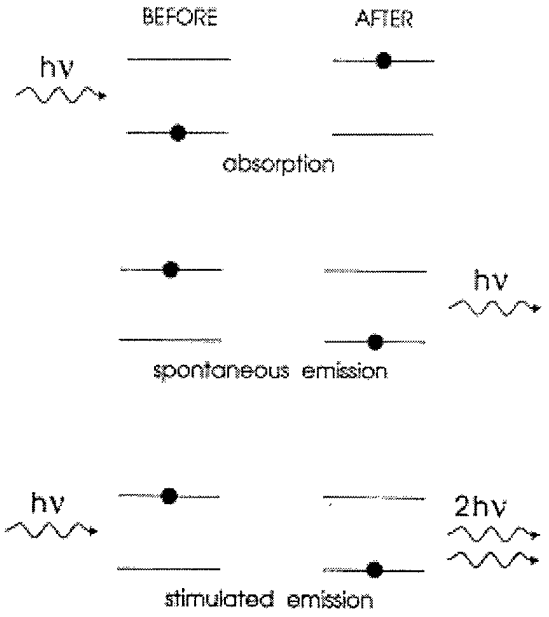

Figure 3. Diagram of the 3 processes that can change the energy state of a molecular system: absorption of radiation, spontaneous emission of radiation, and stimulated emission by radiation. (Bernath: 1995).

It is appropriate to note here that there is no conflict between quantum mechanics and classical mechanics. The laws of quantum mechanics clearly apply to the nuclear and molecular levels of magnitude. As systems of molecules increase and approach the size of what we interact with in life, the resulting quantum levels are at such a large scale that changes from one to another level appear smooth. When this is true, then we have crossed into the arena of classical physics. This is known as the Correspondence

Principle. Succinctly, it states that quantum systems go over to classical behavior in the limit of large quantum numbers (Brown: 1998).

In this research, the rotational temperature of OH was to be determined from the collected spectra. Therefore, a word on the various types of molecular motion is in order. Vibrational motion for a diatomic molecule is defined to be the variation on the internuclear separation whereas rotational motion is the change in orientation of the molecule in laboratory-fixed space. It is shown empirically that the separation between vibrational levels is much larger than that between rotational levels (Brown: 1998). Therefore, the vibrational frequencies are larger than the rotational frequencies. The total energy of the molecule is a sum of the contributions from the electronic, vibrational, and rotational energies:

$$E_{tot} = E_{el} + E_{vib} + E_{rot}. \quad (6)$$

The hierarchy of energy levels is that every electronic level contains many vibrational levels, which in turn contain several rotational levels. The orders of magnitude of the energy levels are such that

$$\Delta E_{el} >> \Delta E_{vib} >> \Delta E_{rot} \quad (7)$$

Translation is an additional type of molecular motion. However, the science of spectroscopy studies translations that occur within individual molecules, each of which is moving at a translational velocity. The primary effect that translational motion has on the observed transition frequency is a small one through the Doppler effect. Also, by referring all coordinates to the molecular center of mass, the three coordinates X, Y, and Z define the instantaneous position of that center and therefore are themselves the translational coordinates.

2.3 Gravity Wave Background

Quantifying gravity wave activity was the ultimate objective of this experiment. Therefore, an understanding of what gravity waves are was needed. The first section below is the discussion of their importance and their creation. The following section deals with the basic physics of gravity wave activity.

2.3.1 Description of Gravity Waves

A gravity wave is a wave in a fluid where the restoring force is gravity. They are fundamentally important to the mesoscale dynamics of the Earth's atmosphere. Gravity waves transport significant amounts of energy and momentum. They trigger convective storms and generate clear-air turbulence. They interact strongly with one another, and in the process, they drive major spectral energy transfers in the atmosphere.

The onset of convective instability in the atmosphere triggers a wide range of atmospheric responses, to include the generation of gravity waves. However, under most times and circumstances the atmosphere is stably stratified. There are waves in the atmosphere at all scales from micro scale to global scale. The mesoscale consists of a time scale of less than several hours and of a spatial scale of a thousand kilometers. In the mesoscale, the earth can be considered locally flat with a relatively slowly rotating, incompressible atmosphere (Hooke: 1986). In the mesoscale, the only preferred direction is the vertical, since the atmosphere has no real upper boundary.

The restoring force of internal gravity waves is buoyancy, which results from the gravitational force and any stratified atmospheric stability. Another class of gravity waves, called inertio-gravity waves, is due to the combined effects of buoyancy and the

Coriolis effect. This class of gravity waves is generally affected to some extent by the rotation of the earth (Andrews: 1987). Atmospheric gravity waves can exist only when the atmosphere is stably stratified so that a fluid parcel displaced vertically will undergo buoyancy oscillations. The atmosphere is a fluid that has no upper boundary. As such, gravity waves may propagate vertically as well as horizontally. In these vertically propagating waves the wave phase is a function of height. Such waves are called internal gravity waves. They are believed to be an important mechanism for transporting energy and momentum to high levels, and for the formation of clear air turbulence (Holton: 1992).

Gravity waves can be excited by atmospheric instabilities or by external forcing like that affecting airflow over irregular terrain. Waves that arise from atmospheric shear instability, or that are generated by penetrative convection of cumulus and cumulonimbus clouds, are responsible for much of the clear-air turbulence encountered by jet aircraft (Hooke: 1986). Gravity waves generated by the airflow over mountains often produce downslope windstorms known as chinook or foehn waves.

Gravity waves modulate every atmospheric variable, including wind speed, temperature, density, etc. As a result, every sensor of atmospheric variables reveals wave motions in the records, to a degree. Gravity waves are not isolated events that occur in a few cases; they are ubiquitous.

Gravity waves perform essential dynamical roles in the atmosphere. These include the following, which are discussed in the next few paragraphs: spectral energy transfer, vertical and horizontal transport of momentum and energy from one region of

the atmosphere to another, generation of the clear-air turbulence that affects aircraft, and triggering of instabilities that lead to the development of severe weather (Hooke: 1986).

Gravity waves, through turbulent spectral energy transfer, provide the initial breakdown of atmospheric momentum and energy from the synoptic scale down to the microscale. This turbulent spectral energy transfer is generally from larger scales to smaller scales, however, it has not been ruled out that upscale energy transfer may be possible during certain forms of shear instability (Andrews: 1987).

Gravity wave transport of energy and momentum occurs in the horizontal and the vertical direction. In the horizontal, it competes with Rossby waves in the movement of energy and momentum. In the vertical, waves of a frequency greater than the buoyancy frequency are evanescent. The buoyancy frequency N (also called the Brunt-Vaisala frequency) has for average tropospheric conditions a value of $1.2 \times 10^{-2}\ s^{-1}$ with a period of oscillation of about 8 minutes. Their energy remains trapped at the height of generation. Waves with a period greater than N propagate their energy nearly horizontally, with slight vertical displacement. When a wave's frequency is approximately equal to N, it is free to propagate its energy vertically (Holton: 1992). However, gravity waves transport a large amount of energy and momentum into the stratosphere. 25% of the vibrational energy in the thermosphere has been determined to originate from gravity waves from the troposphere.

Gravity waves are the predominant cause of clear-air turbulence. Some of this turbulence originates from local shear instability. However, a large portion of the turbulence is generated from nearby convective storms, which force oscillations into the stable environment.

Also, gravity waves can be the trigger that initiates convective activity. By modulating the atmospheric stability, convective instabilities are then able to overcome weakened areas such as capping inversions.

2.3.2 *Basic Physics of Gravity Waves*

Internal gravity waves are transverse waves in which the parcel oscillations are parallel to the phase lines as shown in figure 4. A parcel displaced a distance δs along a line tilted at an angle α to the vertical as shown in the figure will undergo a vertical displacement $\delta z = \delta s \cos \alpha$. The vertical buoyancy force per unit mass for this parcel is just $-N^2 \delta z$, where N is the buoyancy frequency. Therefore, the component of the buoyancy force parallel to the tilted path along which the parcel oscillates is just

$$-N^2 (\delta s \cos \alpha) \cos \alpha = -(N \cos \alpha)^2 \delta s \qquad (8)$$

(Holton: 1992).

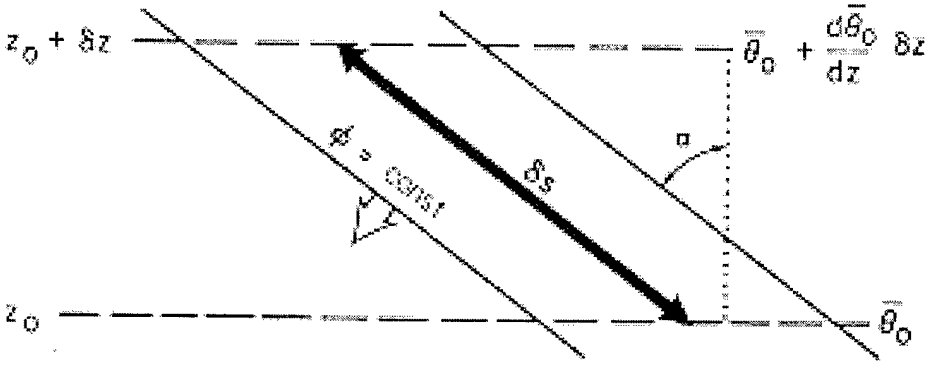

Figure 4. Diagram of a parcel oscillation path (heavy arrow) for pure gravity waves with phase lines tilted at an angle α to the vertical. (Holton: 1992).

Gravity waves of the scale of tens to hundreds of kilometers in horizontal wavelength (not affected by Coriolis) appear to be common in the upper mesosphere, where radars and other instruments have detected them. Figures 5a and 5b show some actual radar observations of internal gravity waves in the mesosphere (Andrews: 1987). The periods of waves of this type are typically a few minutes to an hour, and vertical wavelengths range from 5 to 15 km. Direct measurements are difficult, but the waves are thought to have horizontal wavelengths of up to 100 – 200 km, and horizontal phase speeds of up to 80 m s^{-1}.

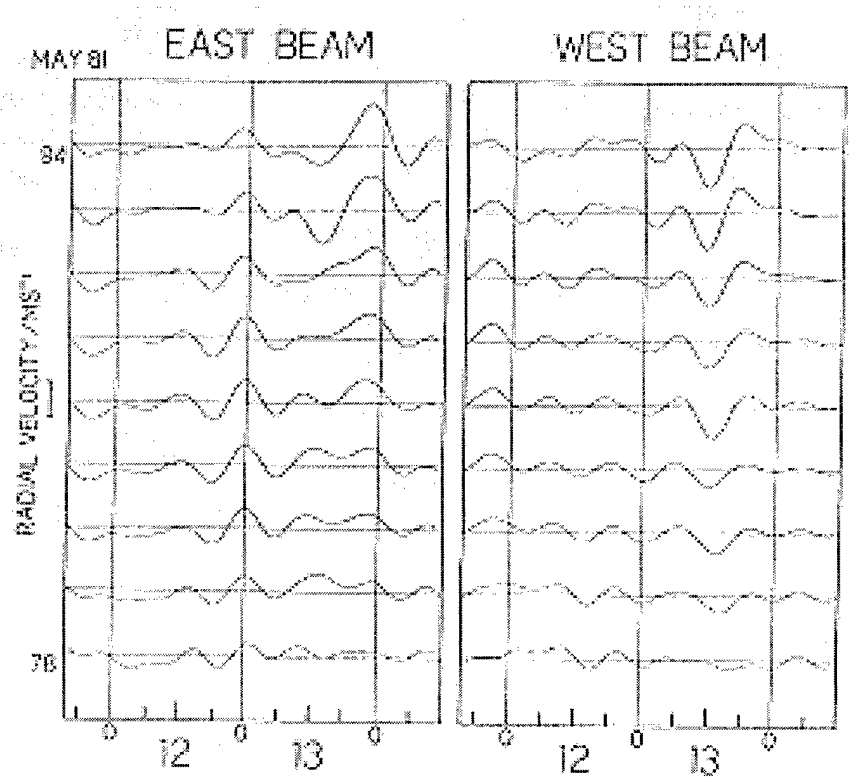

Figure 5a. Graph of vertical movement of gravity waves of periods longer than 8 hours. High frequency radar measurements of line-of-sight velocities at heights between 78 and 94 km in the upper mesosphere measured in two directions, equally inclined at small angles to the vertical. The data were collected during May 11-14, 1981. (Turnbull & Lowe: 1991).

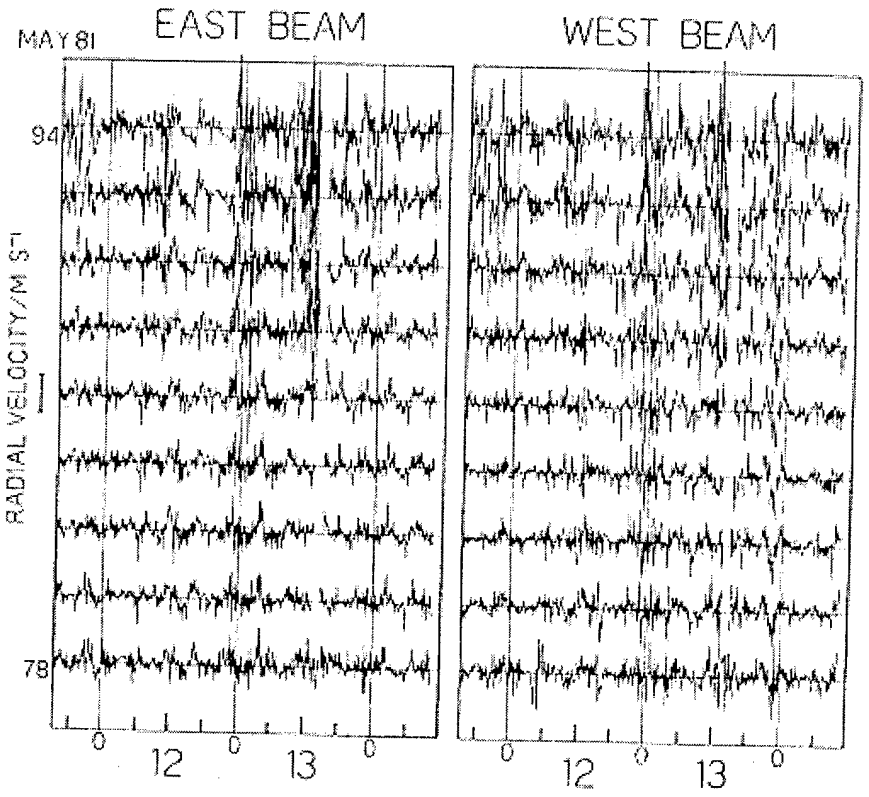

Figure 5b. Graph of vertical movement of gravity waves of periods from 8 minutes to 8 hours. Compare with figure 5a. (Turnbull & Lowe: 1991).

Inertio-gravity waves have periods approaching the inertial period of $2\pi f^{1}$ and vertical wavelengths on the order of 10 km (Holton: 1992). The f is for the Coriolis parameter, which is $2\Omega\sin\varphi$, with Ω being the angular speed of the rotation of the earth ($7.292 \text{ X } ^{10\text{-}}5 \text{ rad } ^{s\text{-}1}$) and φ being the latitude in radians. These waves have been detected in the upper mesosphere and also in the lower stratosphere, and can have horizontal wavelengths of over a thousand kilometers.

Internal gravity waves are also likely to be common in the lower mesosphere and the stratosphere, but observations at these levels are sparse at present (Andrews: 1987).

In this research, it is the internal gravity waves passing through the lower mesosphere that are to be measured.

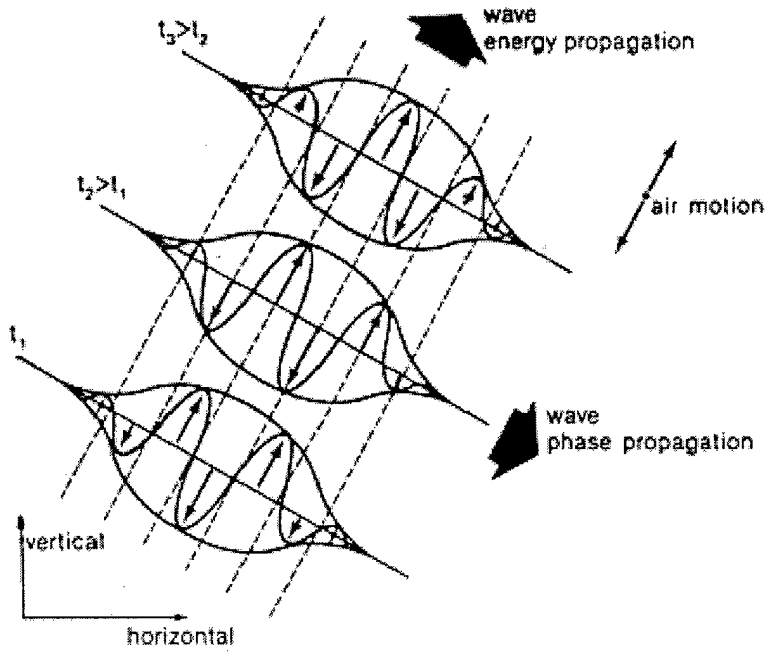

Figure 6. Diagram of gravity wave energy and phase propagation. (Hooke: 1986).

Figure 6 shows the propagation of phase and energy by a gravity wave in a shearless and isothermal atmosphere. As evident in this figure, the effect of the wave generation is to produce shears. This nature of gravity-wave phase and energy propagation is important in wave generation by convective systems, as shown in figure 7. A large thunderstorm acts as a point source of gravity waves when it encounters stable overlying air, often the stratosphere. Short-period gravity waves are observed above the thunderstorm. Longer-period gravity waves are observed at farther distances. Waves

generated in this method are dispersive. Because of this dispersion pattern, the wave frequency is directly tied to the angle of wave propagation relative to the vertical.

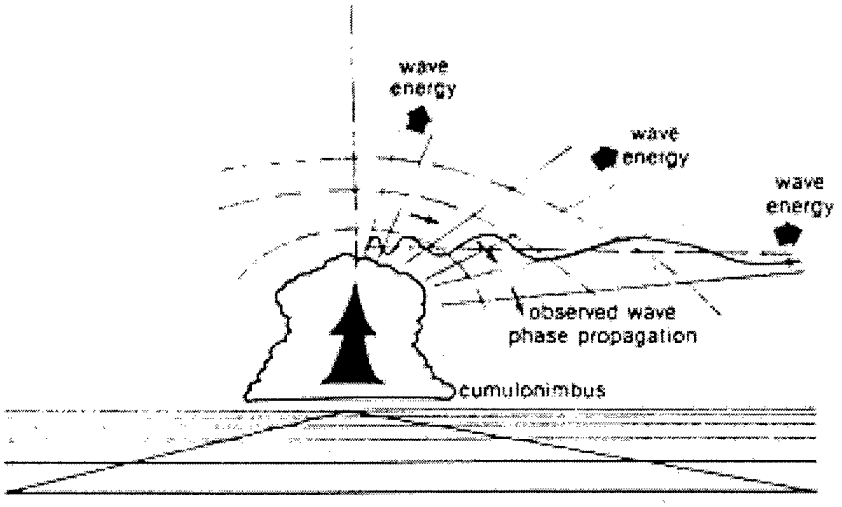

Figure 7. Diagram of gravity-wave generation by penetrative convection. (Hooke: 1986).

Gravity waves are generated by shear instability, or by external forcing. In the case of shear instability, energy of shear flow is converted into wave energy contained in fluctuations in the wave field. The layer is statically stable, but the shear-flow fields may have sufficient kinetic energy differentials across the shear zone itself. In that case, the air parcels can extract some of this available kinetic energy and accelerate away from their equilibrium position once displaced vertically. The Richardson number is a stability index, which states that

$$Ri = (g/T)(\Gamma_d - \Gamma) / (d\mathbf{V}/dz)^2 = N^2 / (\partial \mathbf{V}/\partial z)^2 \qquad (9)$$

where N is the Brunt-Vaisala frequency, $\partial V/\partial z$ is the critical shear (vertical wind shear), Γ is the environmental lapse rate, and Γ_d is the dry adiabatic lapse rate (Wallace & Hobbs: 1977). A Richardson number less than ¼ is necessary for turbulence and unstable flow (Hooke: 1986).

External forcing can be either thermal forcing or dynamical forcing, or a combination of the two. Airflow around or over cumulus clouds or thermal plumes launches gravity waves in the surrounding stably stratified air. Airflow over mountainous terrain forces vertical motion of the parcel involved. Airflow over differentially heated areas, such as land-sea boundaries, induces similar circulation patterns. Wave-wave interaction is another important wave source in some regions of the spectrum.

2.4 Hydroxyl Background

The intense near-IR emissions in the nighttime airglow were first identified by A.B. Meinel (1950) as arising from OH overtone transitions. Subsequent investigations using both ground and rocket-based spectrometers have established that the relative populations of the lower rotational levels of OH observed in the nightglow have an approximate Boltzmann distribution. The altitude dependence of the airglow had been measured by fitting the OH emission to its blackbody equivalent assuming a Boltzmann distribution of rotational states where the characteristic temperature is typically found to be near that of the mesopause, which is ≤ 225 K (Smith et al: 1992).

Airglow is defined as a relatively steady, faint photochemical luminescence in the upper atmosphere (Webster's Dictionary). Nightglow is merely airglow at night, thereby

removing the dominant radiation in the atmosphere, which is sunlight. These emissions from the sky, not all of which are visible, include those from OH molecules. A layer of hydroxyl molecules in the mesosphere has a peak concentration at about 87 km altitude with a full width at half peak of 6 to 10 km. The vibration-rotation bands of the hydroxyl radical are the strongest features of the nightglow spectrum, the total emission being about 1 megarayleigh (Turnbull: 1982). A rayleigh (R) is defined as absolute intensity or surface brightness expressed in millions of photons per second per column cross-sectional area (cm squared) along a line-of-sight.

The hydroxyl nightglow is known to result from the process

$$H + O_3 \rightarrow OH\ (v' < 10) + O_2 \qquad (10)$$

where v' is the vibrational level (Lowe: 1996). This creation of OH has been well studied in the laboratory.

Since relatively few studies have been performed on the mesospheric hydroxyl airglow, there remains considerable doubt as to all the details of the excitation mechanism and the possible roles of chemical and collisional quenching. For example, the rate of chemical quenching process

$$OH\ (v_2') + O \rightarrow H + O_2 \qquad (11)$$

has not been determined as a function of vibrational level v'. Rates for the quenching of OH by M where M is O_2 or N_2,

$$OH\ (v_1' = v_2') + M \rightarrow OH\ (v_1' = v_2' - 1) + M \qquad (12)$$

has been measured for $v' = 5$ to 9 (Streit & Johnson: 1976), but the results have been questioned. Also, there have been no laboratory studies of whether the secondary excitation process

$$HO_2 + O \rightarrow OH\ (v' \leq 6) + O_2 \qquad (13)$$

actually produces vibrationally excited hydroxyls or not (Turnbull: 1982).

Formula 10 above is the main destruction process for ozone at night near the mesopause. In equilibrium the rate at which it proceeds is just the rate of formation of ozone through the three-body recombination of atomic oxygen (where M is a catalyst)

$$O + O_2 + M \rightarrow O_3 + M. \qquad (14)$$

Apart from a correction for the effects of collisional quenching, the volume emission rate of the hydroxyl airglow is proportional to the rate of recombination. The origins of any local time variations could be seasonal, tidal, chemical, or a combination of all three. Figure 8 shows a post-twilight decay of the volume emission rate of OH that is believed to be mostly from the chemical process of formula 11 above. Above the altitude of 86 km, the lifetime of atomic oxygen exceeds 24 h so that no significant change in the altitude profile during the night is expected (Lowe: 1996).

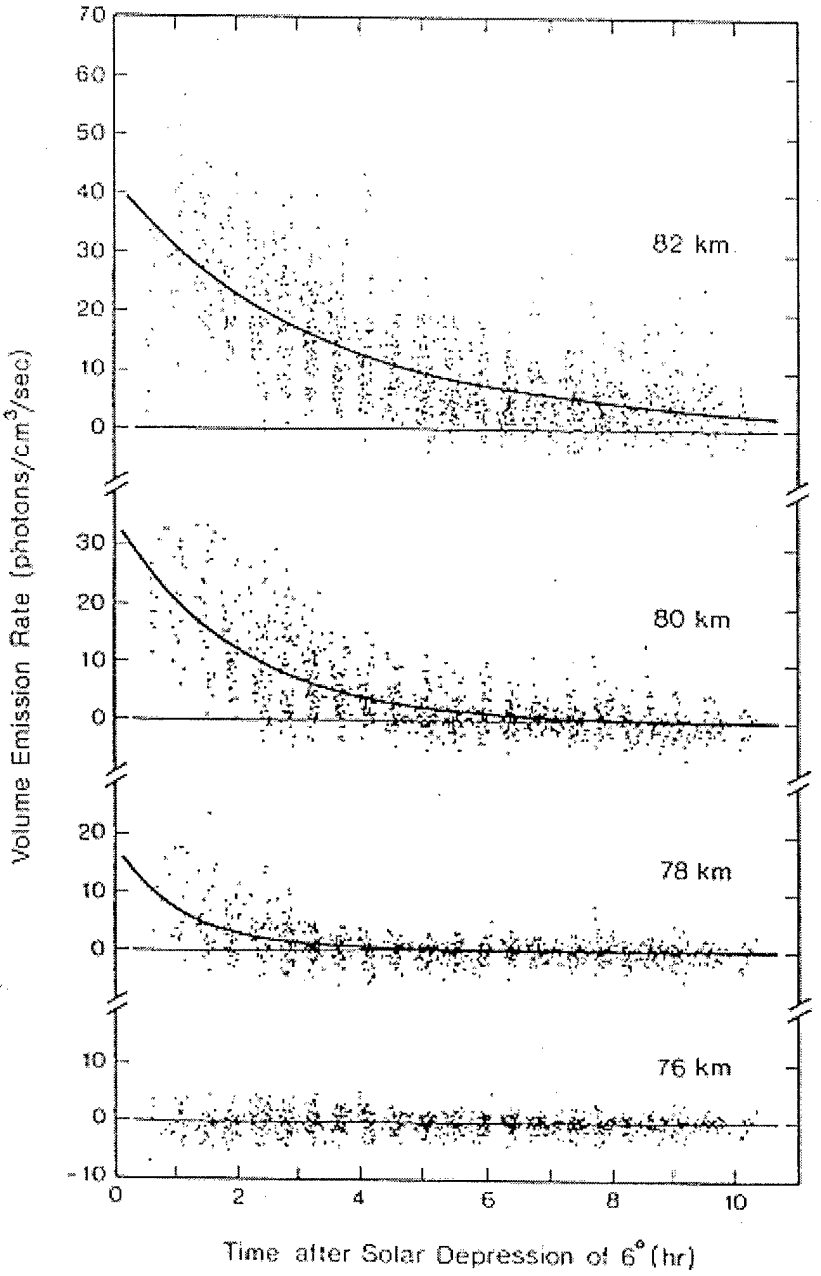

Figure 8. Graph of the evening twilight decay of volume emission rate of the (8-3) hydroxyl band in the 40 ° N latitude band. Each point corresponds to a single measurement made during the period 12 Feb 93 to 26 Apr 93. The solid line is the least-squares best fit of an exponential decay. (Lowe et al: 1995)

2.5 *Previous Studies*

Great advances in nightglow research have been made over the past several decades. Meinel in 1948 deduced the atmospheric emissions as originating from OH. His technical writings are the foundation for all hydroxyl research since.

In 1991 a U.S. space shuttle experiment obtained high-resolution spectral data representing pure OH rotational transitions in the airglow. Emissions from rotational levels as high as N=33 were observed.

Shortly thereafter, a polar-orbiting satellite with instrumentation known as WINDII performed a two-month study of the atmospheric OH spectra. This experiment studied diurnal and possibly some seasonal variations in both the emission rate and the growth of the OH layer in the atmosphere.

Finally, the GLO space shuttle experiment of 1995 is discussed. This is the most recent space-based spectral measurement of the OH nightglow. This experiment has cast considerable doubt on the previously popular view that atmospheric tides dominantly regulated the growth and decay of the hydroxyl layer in the mesosphere.

2.5.1 *Meinel study*

The first discovery of the OH spectrum was performed by A.B. Meinel in 1948. High-resolution spectra of the infrared night sky obtained were determined to be conclusive evidence that previously unidentified infrared emissions were due to the rotation-vibration spectrum of OH.

Meinel obtained spectra using a grating monochrometer. The aspherical corrector plate was replaced by a fused-quartz corrector, which reduced the chromatic aberration of

the corrector. An achromatic collimator was added to the monochrometer. It had an aperture of 6.5 inches and a focal length of 96 inches. The image size, determined visually, was less than 10 μm. Photographic star images as small as 12 μm had been obtained on camera film emulsions (Eastman III-C). Images of stars were taken to give a quantitative feel of the sensitivity of the instrumentation. The monochrometer was mounted on the base of a Navy searchlight. The image of the sky was projected on the slit of the monochrometer by means of a short-focal-length lens. All of the optical elements were coated with magnesium fluoride for low reflection.

High-resolution spectra of the night sky were obtained with a relatively short exposure. Exposure times employed were between 4 - 12 hours. Prior to taking spectra the emulsion plates were bathed in a water, alcohol, and ammonia solution, rinsed in alcohol, and dried. Calibration was done with a tungsten-lamp spectrum.

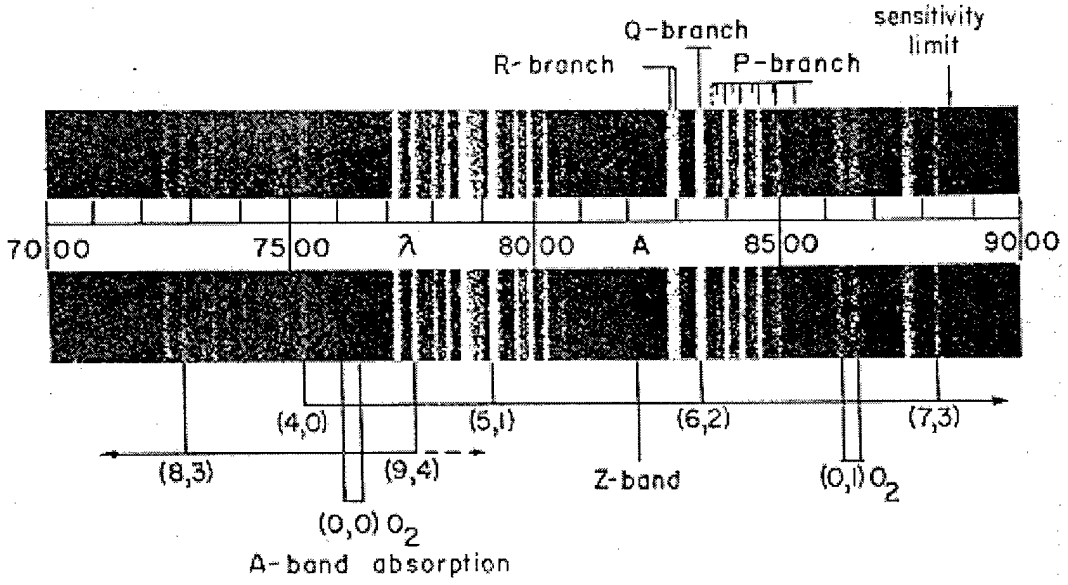

Figure 9. Infrared spectrum of the night sky, 7000-9000 Angstroms (700-900 nm). (Meinel: 1950)

A plate of the spectra, shown in figure 9, clearly shows the detailed structure of each of the OH absorption bands. Wavelengths of the absorption bands were measured from 725.14 nm to 896.22 nm, which includes the primary range of OH emissions that were searched for in this thesis (820-880 nm). It was determined that the actual rotational structure of bands was being shown. Vibrational structure was also determined, and both are listed in table 1.

Table 1. Computed and Observed band positions for OH. (Meinel: 1950).
v' is a rotational level, v" is a vibrational level, λ is wavelength.

Band (v', v")	λ (Comp) (nm)	λ (Obs) (nm)	Band (v', v")	λ (Comp) (nm)	λ (Obs) (nm)
(4,0)	752.6	752.9	(7,3)	885.0	882.9
(5,1)	792.0	791.8	(8,3)	729.3	728.4
(6,2)	836.0	834.7	(9,4)	776.2	775.6

2.5.2 CIRRIS 1A Space Shuttle Experiment

Pure rotation line emissions from highly rotationally excited OH were observed between 80 and 110 km in height as a limb measurement under both nighttime and daytime quiescent conditions (Smith et al: 1992). Data were obtained using the cryogenic CIRRIS 1A interferometer, operated on the Space Shuttle. Transitions from OH with vibration levels of v'=0-2 and rotation levels of v"≤33 were identified between 400 and 1000 nm, corresponding to states with wavenumbers as high as 23,000 cm^{-1}. These measurements dealt with analysis of high rotational level OH emissions, which cannot be described by a Boltzmann distribution. The high-resolution spectral data obtained by the interferometer is the first to represent OH rotation transitions in airglow

at that high of a wavelength. Emissions from rotational levels as high as v"=33 were observed.

The primary instrument was a liquid helium cooled Michelson interferometer with a spectral resolution of less than 1 cm^{-1}. The focal plane contained an array of five arsenic-doped silicon detectors of differing sizes and sensitivities to provide coverage over a wide dynamic range. Ambient airglow was observed under daytime and nighttime. Data gathered were obtained over a spectral range of 400 cm^{-1} to 1250 cm^{-1}. Figure 10 is a sample of the data gathered.

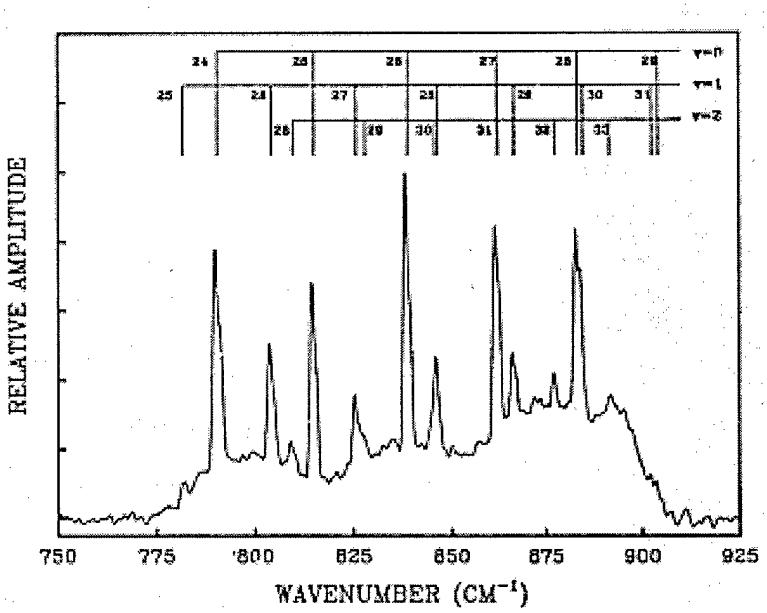

Figure 10. Pure rotation OH spectrum observed in the nighttime airglow from space by the CIRRIS 1A space shuttle experiment. (Smith et al: 1992)

The research onboard CIRRIS 1A deals with high-resolution spectral data that the research of this thesis document could not possibly reproduce; the sensitivity of the

ground-based instrumentation used in this thesis was not expected to be that strong. The sharp features shown in figure 10 were weaker by a factor of ten in spectra obtained under sunlit conditions. It was also found that the hydroxyl rotation-vibration emissions observed at the Meinel bands (550-900 nm wavelength) show a similar strong diurnal variation. In addition, standard atmospheric models predict an order-of-magnitude diurnal variation in the total OH concentration.

2.5.3 WINDII/UARS

A study of measurements taken by the Wind Imaging Interferometer (WINDII) on board the Upper Atmosphere Research Satellite (UARS) provides detailed information of the OH region in the mesosphere (Lowe: 1996). The polar orbiting satellite took measurements from space downward, whereas the research done during this thesis was to measure through the atmosphere from the ground up. The WINDII/UARS research was conducted over a two-month period in the spring of 1993 between 35 ° and 45 ° north and south latitudes. The main objective was to measure wind profiles in the region of the mesopause by determining the Doppler shift of the hydroxyl nightglow emission lines. Additionally, OH profiles were made from the emission rates of the airglow over time.

WINDII observed the hydroxyl nightglow through filters that isolated different features of the (8-3) vibration-rotation band of OH centered on the $P_1(3)$ line at a wavelength of 734.6 nm. The fraction of the total band intensity represented by the $P_1(3)$ line depends on the temperature of the emitting layer. The variation of the range of temperatures from the OH is small since the line lies near the maximum of the Boltzmann

distribution. Therefore the volume emission rate of this line can be used in place of the total volume emission rate with negligible error.

Much of the results from the study of the WINDII/UARS data are relevant to this thesis. In this space-based experiment a peak height of maximum OH concentration was found at 88 km with a total volume emission rate of 35 to 45 photons/cm^3/s for the entire spectrum. Above the peak, the emission falls off uniformly, reaching 10 photons/cm^3/s near 95 km. Below the peak, the decrease is more rapid, with very little emission below 82 km. The width of the peak (full width at half maximum) is in the range 6-9 km.

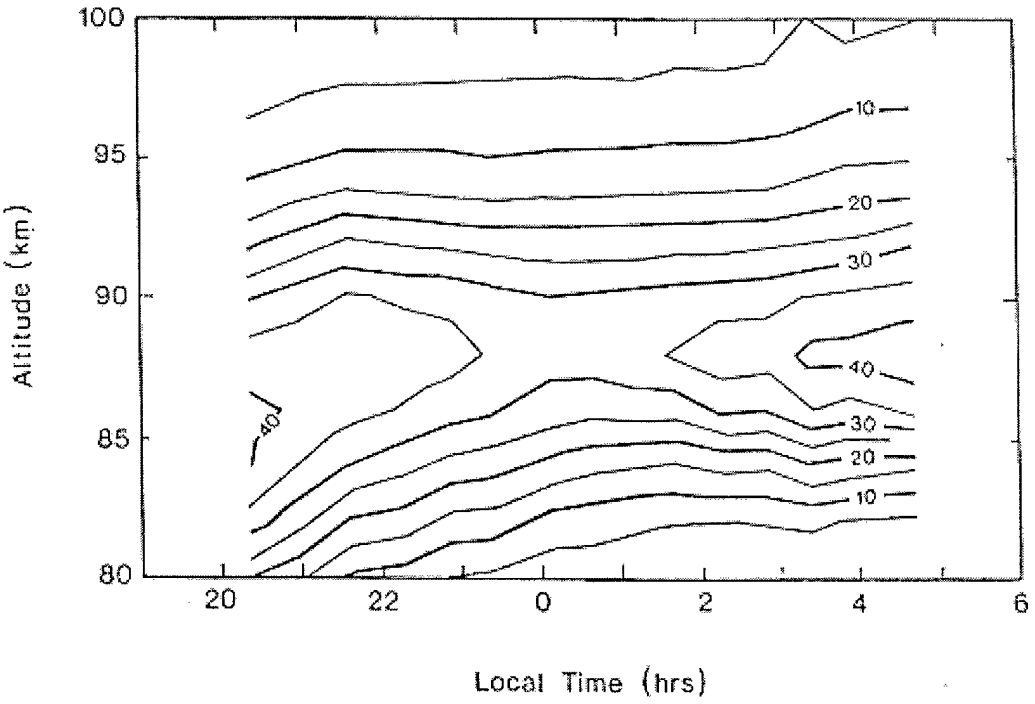

Figure 11. Contour plot of the volume emission rate of the (8, 3) hydroxyl band for the latitude band 40° N ± 50°. Contours are labeled in units of photons/cm^3/s. Data from the period 12 Feb 93 to 26 Apr 93 are included. From the WINDII/UARS observations. (Lowe et al: 1996)

The most significant local time variation occurs during the pre-midnight period at altitudes below the peak of the emission, as shown in figure 11. For example, the 10 photon/cm^3/s contour lies below 80 km at 2000 h local standard time but climbs to nearly 83 km after midnight. The main feature of the post-twilight period is the approximately exponential decay in volume emission rate, with the time constant of the decay increasing with increasing altitude (refer back to figure 8). As a result of this decay, the lower limit of the emitting layer, which is below 78 km early in the twilight, rises to 82 km after midnight. A further feature of these data is the variability at a given time that greatly exceeds the noise level as indicated by the 76 km data. This variability is a measure of the zonal variation of the volume emission rate and is typically at least a factor of two on either side of the mean value.

2.5.4 GLO Space Shuttle Experiment

Instrumentation known as the Arizona Airglow Instrument (GLO) was created at the University of Arizona and carried on the Space Shuttle mission STS-53 in September 1995. The instrument was quite large; GLO included nine imaging spectrographs coupled with nine intensified charge-coupled devices (CCDs).

The main objective of the GLO experiment was to measure a large interval of the OH spectrum from mid-ultraviolet to near infrared. The GLO observations from the shuttle recorded the night airglow layer seen edge on at the Earth's limb. The data represents the first simultaneous optical measurements of airglow emissions over the spectral range from 115 nm to 900 nm.

Contrary to other researchers, the night sky intensity variations recorded by GLO do not exhibit any obvious relationship to atmospheric tides. The intensity variations are possibly due to the result of chaotic superposition of upward and downward vertical motions (Bellaire: 1997). However, this has not been proven.

Figure 12 is the night sky spectrum as recorded by GLO. This figure displays the features to look for in this thesis research. Note the large intensity of O_2 at 762 nm. If this O_2 could not be found in spectrum of the night sky, then no OH nightglow would be recorded. Absolute intensity in figure 12 is shown in Rayleigh units. One rayleigh unit (R) is one million photons per second per column cross-sectional area (in cm^2) along the line-of-sight in the atmosphere.

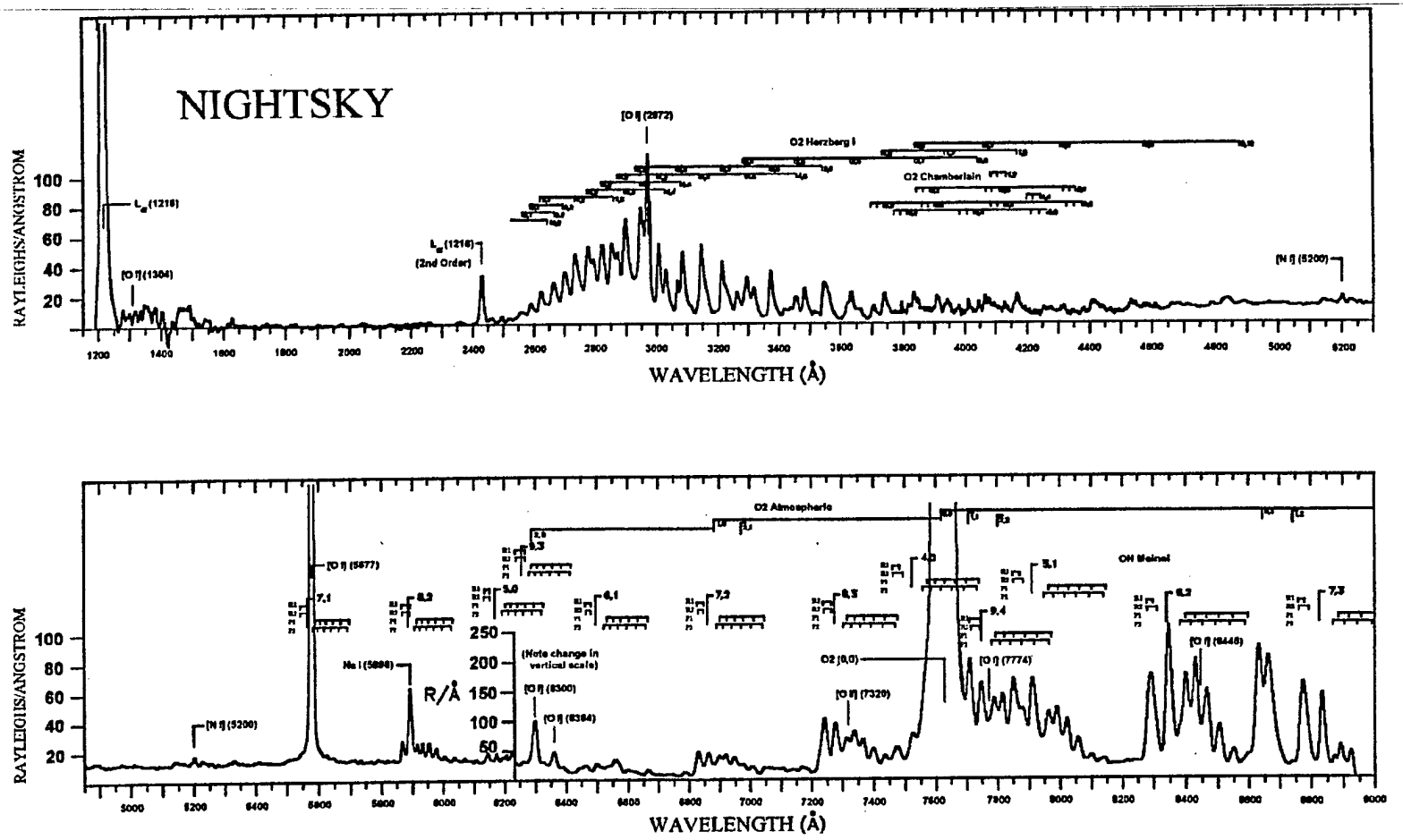

Figure 12. The night sky spectrum as recorded by the Arizona Imaging Spectrograph (GLO) in Sep 95. Wavelength interval is from 115 nm to 900 nm. (Bellair70

III. Hardware

3.1 Overview

Chapter 3 discusses the equipment and their functions in the system used to measure hydroxyl nightglow. Calibration of the system for optimal signal strength is treated separately from the description and configuration of the hardware. Determination of wavelength interval is also covered. Limitations of the optic fiber are discussed in the last section.

3.2 Description and Configuration

In the following subsections, major components of the instrumentation are described to include their capabilities and functions.

3.2.1 Telescope

The purpose of the telescope was to passively collect the radiation from the night sky, then focus it down to the size of the optic fiber opening. The telescope was a Meade 12-inch LX200 Schmidt-Cassegrain that had a 305 mm diameter and focal length of 3048 mm. (See figure 21 of the appendix). The eyepiece usually used on the telescope was removed. The eyepiece was replaced by a metal cylinder containing a focus lens. The cylinder focuses the signal onto the connected optic fiber. A field tripod stabilizes the telescope.

The power of the telescope was 117.2X magnification, which was the focal length of the scope (3048 mm) divided by the focal length of the eyepiece (26 mm). The

apparent field of view was 0.44 degrees. This was determined by the field of view of the eyepiece (listed as 52 degrees) divided by the magnification.

3.2.2 Optic Fiber

The purpose of the 10 ft long optic fiber was to guide the signal collected from the telescope into the monochrometer. One end of the fiber had a 1 mm diameter round opening for receiving the signal from the telescope. The other end had been flattened into a single linear array of smaller fibers creating a slit 4 mm long and 0.2 mm wide. The thin array was necessary for focusing the entire signal into the incoming slit of the monochrometer.

3.2.3 Monochrometer

The purpose of the monochrometer was to take the incoming signal of wavelengths that were mixed together, and separate them into a thin line of radiation ordered by wavelength, i.e. a spectrum. The monochrometer was an Acton Research Corp. (ARC), Spectrapro 275 (figures 23-25 in the appendix). Exposure time could be as small as 0.005 seconds or a multiple of this value. It had a 0.275-meter triple grating system.

The diagram in figure 13 shows the unfiltered beam of radiation enter the monochrometer, pass by a mirror, then pass by a focusing lens to the grating. The grating then spreads the radiation into a wide wavelength-orderly spectrum. This spectrum is then passed to another lens and mirror before leaving the monochrometer and entering the detector.

A grating is similar to a mirror, except that the surface isn't smooth; It has a serrated surface of sharply angled grooves. This is shown in the right portion of figure 13, at an exaggerated scale. The grating is what separates the signal into a spectrum. A 1200 groove/mm grating which was blazed at 750 nm was the primary grating used for measurements. The blaze is the optimum wavelength for which the grating operates. The optimum wavelength range is determined by halving the blaze for the lower end and doubling the blaze for the higher end. Therefore, the wavelength interval of optimum efficiency was 375nm to 1500 nm.

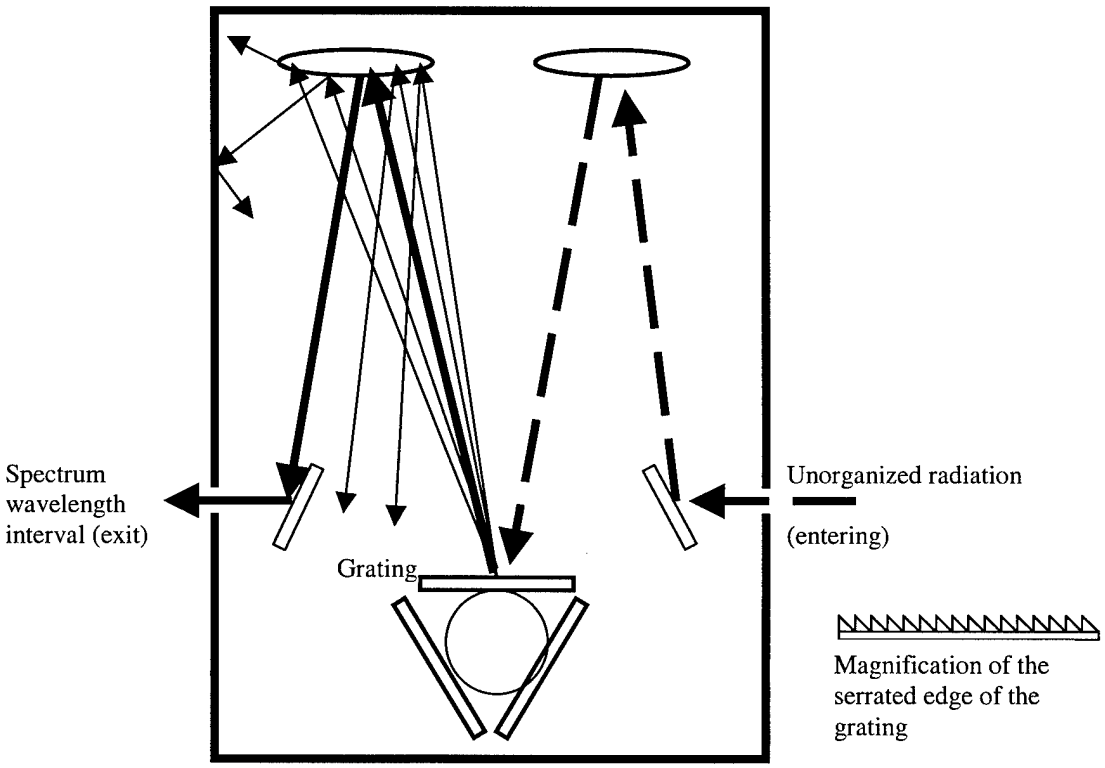

Figure 13. Diagram of a grating monochrometer. The grating spreads the unorganized radiation into a wavelength orderly spectrum. The grating is angled so that only the desired wavelength interval exits the instrument.

As seen in figure 23, a special adapter was attached to the monochrometer that was created for the single array exit of the optic fiber. A mirror within the adapter collimated the signal to the entrance slit of the monochrometer.

When a given wavelength is entered into the attached keypad, the grating within the monochrometer slowly rotates until the desired wavelength of the spectrum is aimed at the exit slit. This wavelength passes through the exit slit and into the detector. All other wavelengths (the ranges not desired) are either angled either too much or too little by the grating. These others remain trapped within the monochrometer (see figure 13).

Although a single wavelength number is entered into the keypad, what is actually received is a wavelength interval, where the desired wavelength is centered on that interval. It is this wavelength range that enters the detector and is ultimately displayed on the computer screen. Further discussion of the interval is in section 3.4 below.

3.2.4 Detector and Controller

The detector and its controller are the ST-121 series from Princeton Instruments. The detector (figure 25) attaches to the exit slit of the monochrometer. The small wavelength interval of radiation exiting the monochrometer illuminates a single array of 1024 photoelectric diodes within the detector. The amount of illumination on each array determines the signal strength of the associated wavelength. This data on wavelength signal strength are continuously streamed through the controller to the computer. The controller processes the data into a data type that the computer can understand.

The detector requires a temperature below –20 °C in order to minimize any internal heating from corrupting the diodes and thereby giving any false signal strength.

Cooling the system also improves the signal-to-noise ratio. A water recirculator (figure 26) pumps water through the detector to remove heat. The recirculator has a heating and cooling system built in. The controller monitors the temperature. When the temperature is too high, the controller instructs the detector to transfer more heat to the water pipe.

The cool temperatures within the detector make it susceptible to fogging and icing of the internal mechanisms and of the diodes. To prevent this, nitrogen gas gently blows into the detector. A standard tank of pressurized nitrogen was used.

3.2.5 Software and Computer

A Dell Optiplex XMT590 with MS-DOS was used for running the CCD Spectrometric Multichannel Analysis (CSMA) software version 2.4a, by Preston Instruments. The data travels from the controller into the computer where the CSMA software displays the wavelength interval on the X-axis and the relative intensity on the Y-axis. Changing the exposure time, number of accumulations, and number of sequential acquisitions can be done within the software. In addition, many processing functions can be performed using the software, to include background subtraction, flat field correction, and mathematical manipulations.

Figure 2 is an example of a spectrum interval displayed on the CSMA software. Note that the Y-axis is actually relative intensity, rather than absolute intensity.

3.3 Calibration

Many steps were taken to calibrate the system. Most calibration techniques were completed using an Oriel mercury pen lamp in the laboratory and without the telescope in the system.

One such task of calibration was the positioning of the outgoing optic fiber in relation to the incoming slit of the monochrometer for maximum signal strength. This was accomplished using the entire system minus the telescope and the focusing cylinder that normally is on the optic fiber. The incoming end of the fiber was held a fixed distance from the pen lamp. The exiting end of the fiber was then rotated or moved in or out of the monochrometer attachment (figure 23). The monochrometer was set to 546 nm where a large line exists on the mercury spectrum. The fiber was moved as little as possible to the human touch. After each movement, a 20-second reading was taken. Each reading was created by 20 accumulations of 1-second exposure times. The relative intensity was noted and the process was repeated until a maximum relative strength was found.

The incoming end of the optic fiber had to be optimally positioned in the focusing cylinder so that the maximum amount of signal would enter the fiber. See figure 23 to see the cylinder and optic fiber coupled. The same calibration technique was used that is mentioned in the paragraph above, except that this time the fiber-monochrometer coupling was kept stationary and the focusing cylinder-fiber coupling was moved as slight as possible.

The grating within the monochrometer was calibrated to ensure that for a given intensity coming into the system, the maximum intensity possible would exit it. The same calibration scheme in the previous paragraph was used. It should be noted that the detector's array consisted of photoelectric diodes that were very sensitive. The intensity of light from a well-lit room is enough to permanently damage the electrodes. Each reading was performed in the lighted room with the mercury pen lamp. After each

reading, all light sources would be turned off or covered up. The top of the monochrometer would then be removed and the turning of screws would be done in the darkness as little as possible. Then the top would be placed in position, and the process would be repeated. The grating has several screws for changing the pitch, yaw, diagonal, and skew. Performing this task resulted in an increase in relative intensity of a factor of 12.

Mirrors within the monochrometer had to be aligned so that the correct wavelength interval was exiting it. This was far easier to accomplish than was the grating alignment. The detector was not needed; it was removed and the lights were left on. A red light Helium-Neon calibration laser was aimed into the incoming slit of the monochrometer. The wavelength 587.5 nm Helium line was entered into the instrument's keypad. The wavelength then passed through exit slit and was marked on a stationary board. This procedure was repeated with the 1175 nm line and again with the 1762.5 nm line. These lines are the resonance lines of the 587.5 nm line; they are the double and triple "reflections" of the original line. A mirror would then be repositioned by a small amount. The process would be repeated until all three marks on the stationary board were at the same point. This calibration resulted in a perfect alignment that was proven by repeating the tests with different Helium lines.

Another calibration was needed to minimize the unequal signal strength of the detector array. This unequal signal strength was discovered while testing the system. Once again, spectra were taken of the mercury pen lamp intensity of the 546 nm line. Each reading was taken with the monochrometer centering on a wavelength a few nanometers above or below the 546 nm line. This way, the intensity line would be within

the wavelength interval displayed, but would be off center. The line appeared to grow in intensity by a factor of 3 from one end of the interval to the next.

Optimally, the intensity should be the same no matter what position it holds within the wavelength interval selected for scanning. The undesired effect was minimized by additional corrections in position made to the grating within the monochrometer, by the technique discussed above.

Once that was done, further improvements were made by changing the alignment of the detector in relation to the monochrometer. Screws on the detector allow it to be rotated while remaining flush with the monochrometer. Three spectra would be taken so that the intensity of the 546 nm line would be determined to the left, right, and center of the interval. In other words, the intensity of the mercury line was measured on the left, right, and center of the detector's diode array. Once the three measurements were taken, the detector would be turned to the slightest touch possible. Repeating these steps multiple times resulted in one side of the diode array measuring just 22% stronger than the other side.

Once all the testing and calibrations were completed that could be accomplished indoors, it was time to test and calibrate outdoors. The couplings of the optic fiber to the telescope and of the optic fiber to the monochrometer were both calibrated in the outdoors at night. The same procedure was done outdoors as was done indoors, except that instead of using a mercury pen lamp, a mercury streetlight was used.

3.4 Determination of Wavelength Interval

As stated above, the desired wavelength entered into the keypad of the monochrometer was actually centered on an interval that was measured. The range of the wavelength interval was determined by the following: The mercury lamp was held at a fixed distance from the optic fiber and several readings were taken. For each reading, the center wavelength was decreased (increased) until the 546 nm line was to the extreme right (left) of the window on the computer. The 546 nm line was at the extreme edges when the monochrometer was centered at 512.5 nm and at 579.5 nm. Therefore, the wavelength interval is 67 nm.

3.5 Limitation of the Optic Fiber

Signal loss via the optic fiber was a prime concern. All radiation from the night sky that entered the telescope would focus down to the optic fiber. The fiber was the transport for the signal into the monochrometer. To achieve the maximum signal possible from the radiation entering the telescope, the monochrometer would have to be directly attached to the telescope. This was not possible due to the instability of the resulting contraption, as well as possible damage to the telescope's star-tracking motors. Therefore, an optic fiber was necessary.

To determine the signal loss due to the optic fiber, the mercury lamp and its 546 nm line were used once again. The lamp was placed 5 cm from the entrance slit of the monochrometer and a measurement was taken. Next, the optic fiber was attached to the monochrometer and the lamp was placed 5 cm in front of the entrance of the fiber. Another spectrum was taken. The ratio of the two resulted in an 11.8% signal loss.

IV. Methodology

4.1 Overview

Calibration and testing of the instrumentation was covered in Chapter III: Hardware. This chapter concerns the pursuit of the collection of hydroxyl nightglow emissions in the field in section 4.2. Section 4.3 discusses what would have been done with the OH emission spectra had they been successfully collected.

4.2 Collection Procedure

The apparatus as described in section 3.2 was assembled outdoors at a country field outside of Xenia, OH far from city lights, which would have interfered with signal strength. Gravity wave activity was to be quantified by measuring the nightly temperature variance. The telescope is pointed to near-zenith in an area of the sky with no bright stars. Calibrating the system for maximum signal throughput was performed as described at the end of section 3.3.

Exposure times of 1 second each with 10 accumulations of exposures were accomplished. Spectra are then taken at 20 and 60 accumulations of 1-second exposures. Exposures of times larger than 1 second (up to 10 minutes) were also performed in an attempt to decrease the noise in the signal.

Experimentally, it was found that large exposure times with few accumulations reduced the noise signal by half as opposed to small exposure times with many accumulations. For example, figure 19 was accomplished using a 60 second exposure and 3 exposure accumulations, whereas figure 20 used a 600 second exposure with no

additional accumulations. The 773nm intensity shown in both images is not visually seen when the same wavelength intervals were taken when using 600 accumulations of 1-second exposures.

The slit width on the incoming end of the monochrometer limits the amount of radiation entering the instrument. If the width is too wide, then a large amount of radiation enters the detector via the monochrometer. The photoelectric diode array within the detector is extremely sensitive to intensity. A large amount of radiation would easily saturate the detector, resulting in a meaningless intensity reading. Too much radiation would permanently damage the diode array. During indoor testing and calibration with the mercury pen lamp 1 cm away from the optic fiber, a slit width of 4 μm would allow mercury lines to be recorded. In the outdoor measurements, a slit width open to maximum size, 200 μm was used in an attempt to gain any nightglow. The intensity readings of figures 18 to 20 were taken at maximum slit width.

Another aspect of slit width is its relation to spectral resolution. The larger the slit width, the greater the amount of radiation impinging upon the diode array in the detector. This decreases the ability of the detector to resolve features. An extreme case is when too much radiation enters the detector and the signal is saturated. The finest resolution obtained using the instrumentation is 0.41 nm of full width at half maximum of any intensity line. This corresponds to the width of 6 pixels in the diode array. This is true whether measuring emissions from the mercury pen lamp in the laboratory or measuring mercury or xenon from streetlamps.

Spectra were taken on 11 cloud-free nights in November and December 2000. Air temperatures were frequently -15° C. Radiational cooling of the earth resulted in

frost build up on the telescope optics. Every five minutes of spectrum measurements was followed by using a hair blow dryer to heat the air next to the objective lens of the telescope to remove the layer of frost that was continually forming. Care was taken to not blow heat directly on the lens, as that would have warped the optics.

Spectrographs were taken of wavelength intervals over the visible and near infrared spectrum from 450 nm to 1150 nm. After each night of no nightglow measurements, the equipment would be taken back to the laboratory. Improvements to the system were made by further calibrations and the changing of different lens inserts at the telescope/optic fiber coupling.

A measurement of radiation in the night sky was recorded by using a single 600-second exposure with slit width at maximum. Through use of a filter, this was proven to not be O_2 or OH. Its identification is still unknown. This is displayed in figures 18 to 20 and discussed further in section 5.3.

Had hydroxyl nightglow spectra been successfully taken, they would have been repeatedly taken over time one after the other. The same exposure and accumulation sequence that was successful would be used for all additional spectra. A wavelength interval that displayed at least three intensity spikes would have been chosen, so that the methods discussed in the pre-processing section (4.2.2) could be accomplished.

4.3 Processing

If hydroxyl nightglow measurements had been taken, the following procedures would have been accomplished. For a Boltzmann distribution of rotational levels, the intensity in photon units of a hydroxyl emission is given by

$$I = [(N'_v A)/Q'_v] 2(2J' + 1) \exp [-hcF(J')/kT_{rot}] \quad (15)$$

where N'_v is the population of the vibrational level v', A is the Einstein transition probability appropriate to the transition, F(J') is the upper state rotational term value, T_{rot} is the rotational temperature, and Q'_v is the rotational partition function (Turnbull: 1982). The equation can be written

$$\ln [I/(2A(2J' + 1)) = \ln [N'_v/Q'_v] - hcf(J')/kT_{rot} \quad (16)$$

so that a plot of the left-hand side versus $hcF(J')/k$ should yield a family of straight lines, one for each vibrational level. The rotational temperature T_{rot} could be determined from the slope of each line. The relative vibrational populations N'_v could be determined from the intercepts.

However, for each spectra taken, there would be (hopefully) three or more wavelength intensities on that wavelength interval for the given time. Because these intensities occurred simultaneously, their temperatures should be nearly the same. For the family of straight lines mentioned above, a least-squares straight line would be found that fits the family of lines. The slope of this single line will be the rotational temperature for that time interval. An example is figure 14.

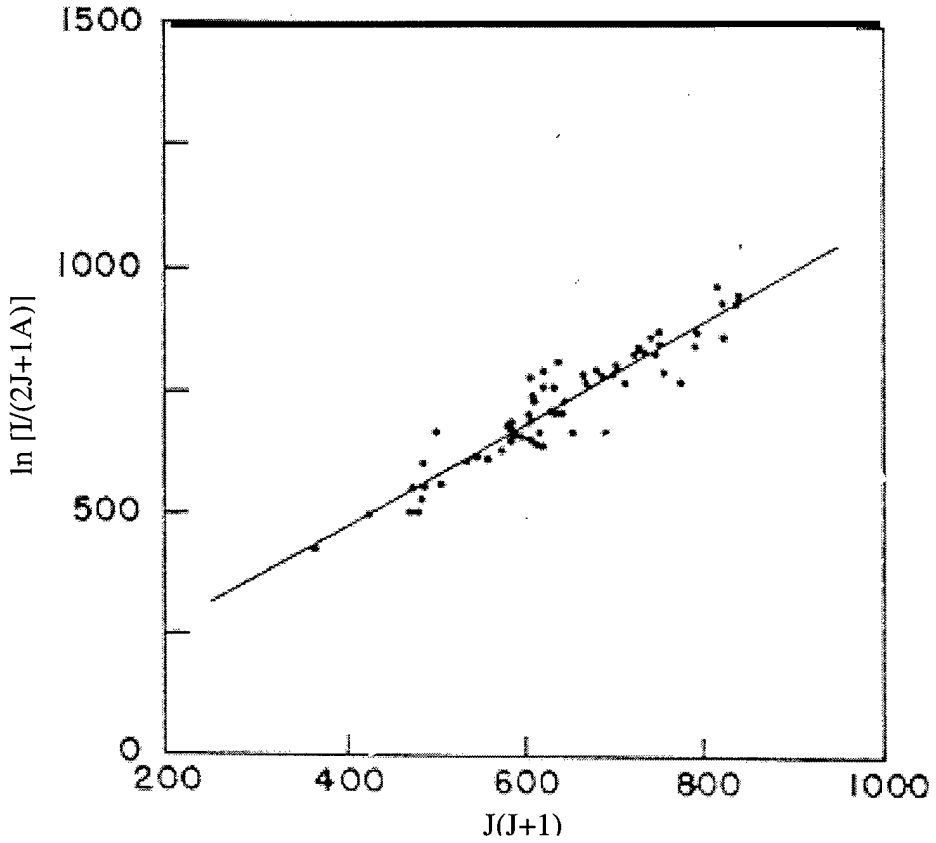

Figure 14. Graph of the intensities of the OH (5,1) band. Each plot is a rotational temperature of an intensity line as derived from the Boltzmann distribution formula (equations 15 & 16). The slope of the regression line is the overall rotational temperature. (Takahashi & Batista: 1981)

Since the spectra are taken one after another, the series of rotational temperatures would be binned into fifteen-minute average values in order to reduce noise. Figure 15 is an example of measured rotational temperature. Variance in temperature would then be determined and plotted as in Figure 16 as a measure of gravity wave activity.

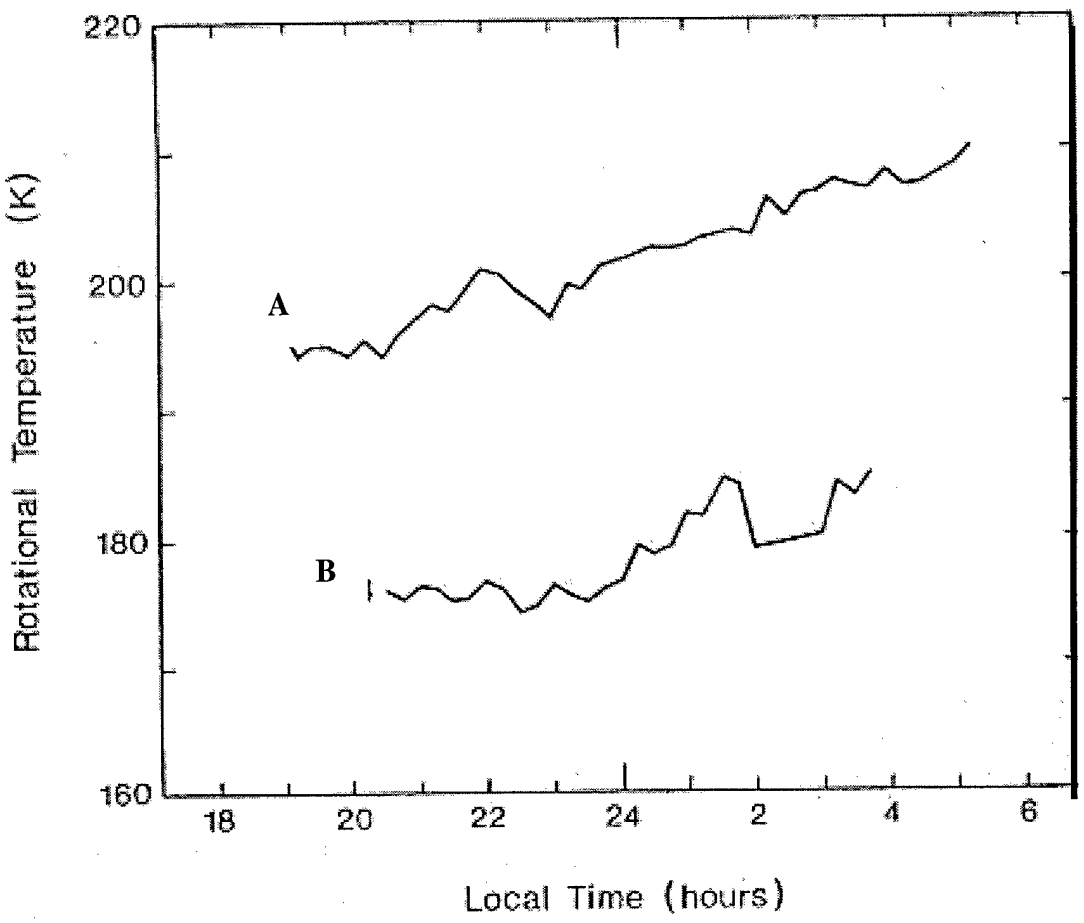

Figure 15. Graph of average diurnal variations. Fifteen-minute time bins of rotational temperature over time. **A** and **B** are of different two different geographic locations. (Lowe & Turnbull: 1995)

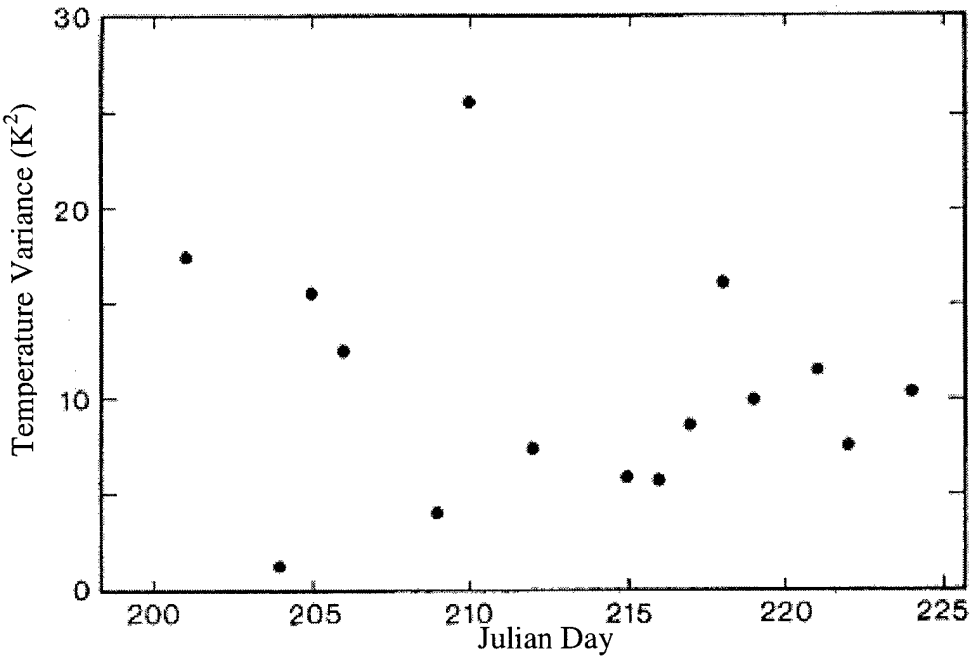

Figure 16. Graph of observed gravity wave activity. The quantity plotted is the temperature variance. (Lowe & Turnbull: 1995)

Diurnal variations would be searched for in the resulting plots. Had any severe thunderstorms been active in the U.S. on nights that nightglow measurements were made, any possible relationship in intensity and proximity of the storm would have been investigated. However, since few supercell and multicell cell thunderstorms occur in November and December, the chances of more than one occurring are slim.

V. Analysis and Results

5.1 Overview

No hydroxyl nightglow was ever detected. As shown in figure 12, diatomic oxygen (O_2) should have given the strongest intensity in all of the atmospheric nightglow at 762 nm. Yet not even O_2 was found in the signal. The resulting signal was flat with the exception of two features discussed in sections 5.3.

The strength of the system and its ability to receive radiation and display a spectrum is shown in section 5.2. Section 5.3 discusses what was detected when searching for hydroxyl nightglow. To test the equipment further, spectra were taken in a laboratory from a plume emission of super conducting film ablated by laser. This test is mentioned in section 5.4.

5.2 Mercury Streetlights Reflected in Clouds

Spectra were taken of mercury streetlights and of xenon lights atop of cellular phone towers. To test the sensitivity of the instrumentation, the system was assembled outdoors and pointed to the zenith on a cloudy night. A solid stratus deck of cloud cover had a base of 5000 ft. The location of the system was in town with many street lamps in the vicinity.

As shown in figure 17, the mercury peaks of 546 nm as well as the double peak found at 577 and 579 nm were detected from the street lamps by reflection of the cloud cover. A wavelength intensity of something being reflected by the cloud cover other than

mercury was detected at 569 nm. Its identification is unknown. When pointing the telescope at a street lamp directly, peak B is absent, but all mercury lines remain.

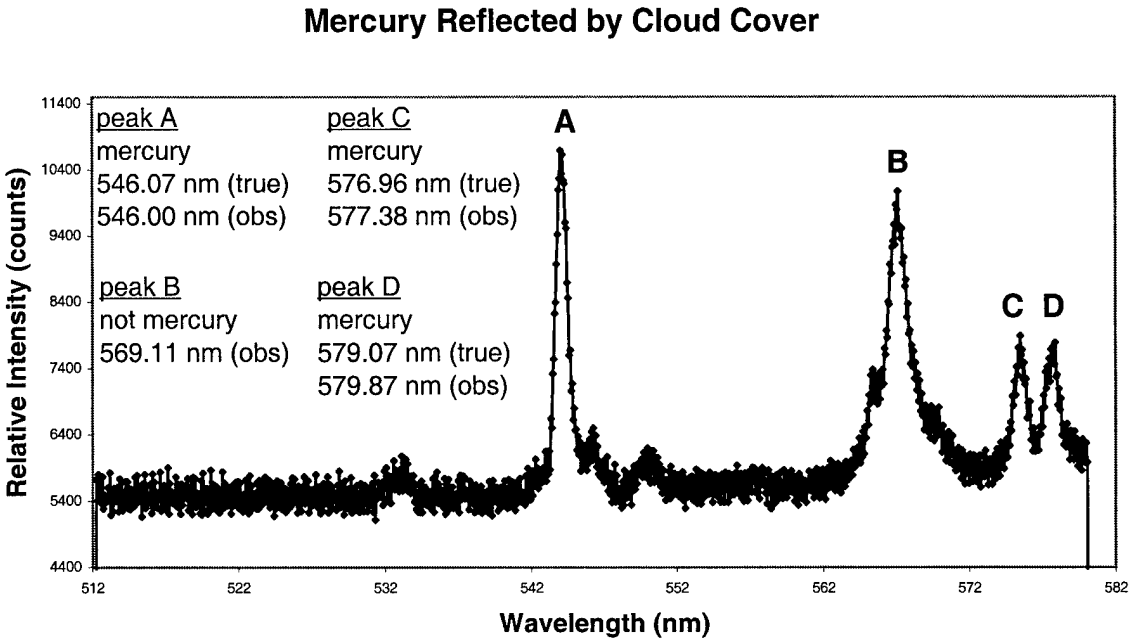

Figure 17. Emission spectrum of mercury reflected by cloud cover centered at 546 nm. Mercury lines are A, B, and C. The telescope was pointed to zenith and measured radiation from street lamps that was reflected by cloud cover. The stratus cloud deck was at 5000 ft. Peak B is not mercury; its origin and identification are unknown. Incoming slit width of the monochrometer is 200 μm with a period of integration of 20 s.

5.3 Attempted Measurement of Hydroxyl Nightglow

For the detection of nightglow, all equipment was assembled in a field outside of Xenia, Ohio, far from city light sources. Measuring the spectrum of a single distant

streetlamp is how the equipment was tested. The telescope was pointed to the night sky and several attempts were made to measure any kind of nightglow, to include the emission from O_2 at 762 nm. Nothing that was expected was found.

When the monochrometer is set at 0 nm, the grating becomes essentially a mirror since no spreading of the signal by wavelength occurs. What results is a single intensity reading of all wavelengths. Figure 18 is such a spectrum. The telescope was pointed at near-zenith away from any bright stars. The moon was not in the night sky. Since this reading is has intensity, then something is being recorded. Another reading was taken, this time with a filter lens mounted between the telescope and the optic fiber. The filter was designed to permit only the 762 nm wavelength to pass through. If OH or O_2 were contributors to the intensity reading in figure 18, then the intensity "hump" would still be present in the spectrum. The result was a reading of no intensity. Therefore, the radiation must be from another source.

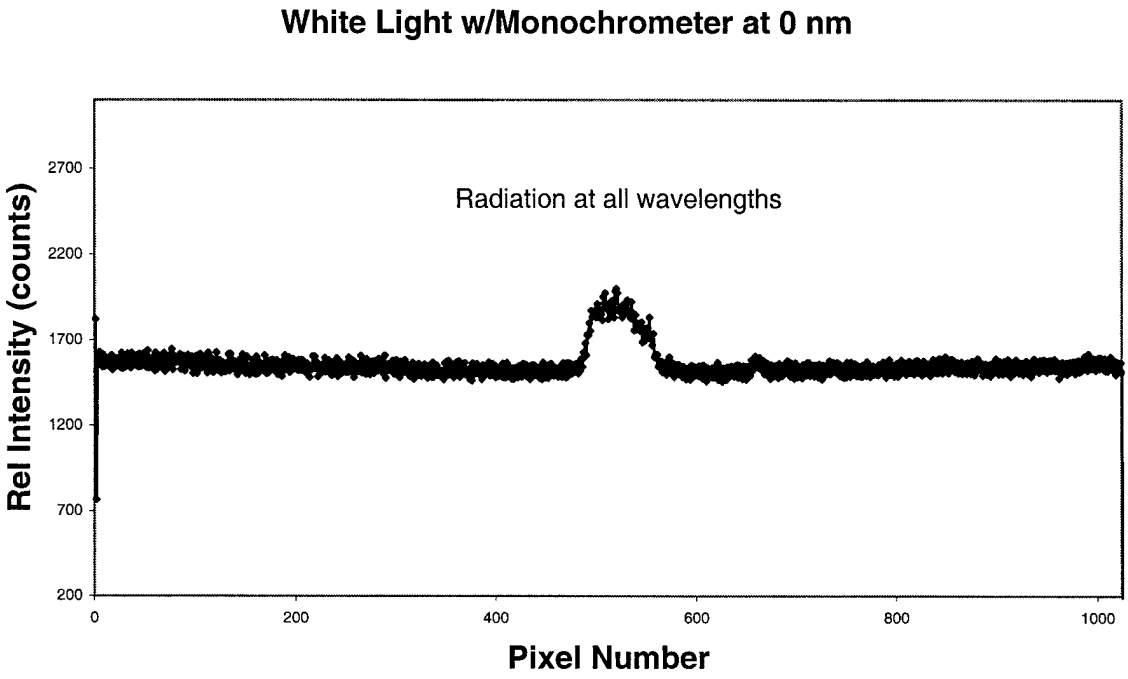

Figure 18. Emission spectrum of all radiation from the atmosphere (as received by the telescope, non-wavelength specific). Monochrometer incoming slit width is 200 μm with a period of integration of 6 minutes. The X-axis does not correspond to wavelength. Figures 19 and 20 show an intensity at 773 nm that contributes to this total amount.

All wavelength intervals were checked from 450 to 1150 nm to find any intensity reading that may be a major contributor to the total intensity of radiation shown in figure 18. A small intensity was found at 773 nm, and is displayed in figures 19 and 20. It is unknown what created this emission. It is not hydroxyl nightglow, however.

Note that the spectra shown in figures 18 through 20 were taken with a monochrometer slit width of 200 μm, in order to capture the maximum amount of incoming radiation. Each of the figures was taken with a 6 minute period of integration.

There is noise inherent to the monochrometer. In figures 19 and 20, the noise is marked with arrows. This noise is a property of the monochrometer itself. The noise is present when taking measurements in the field or in the laboratory, whether or not the telescope or optic fiber are used. Noise is even present when performing blackbody calibrations.

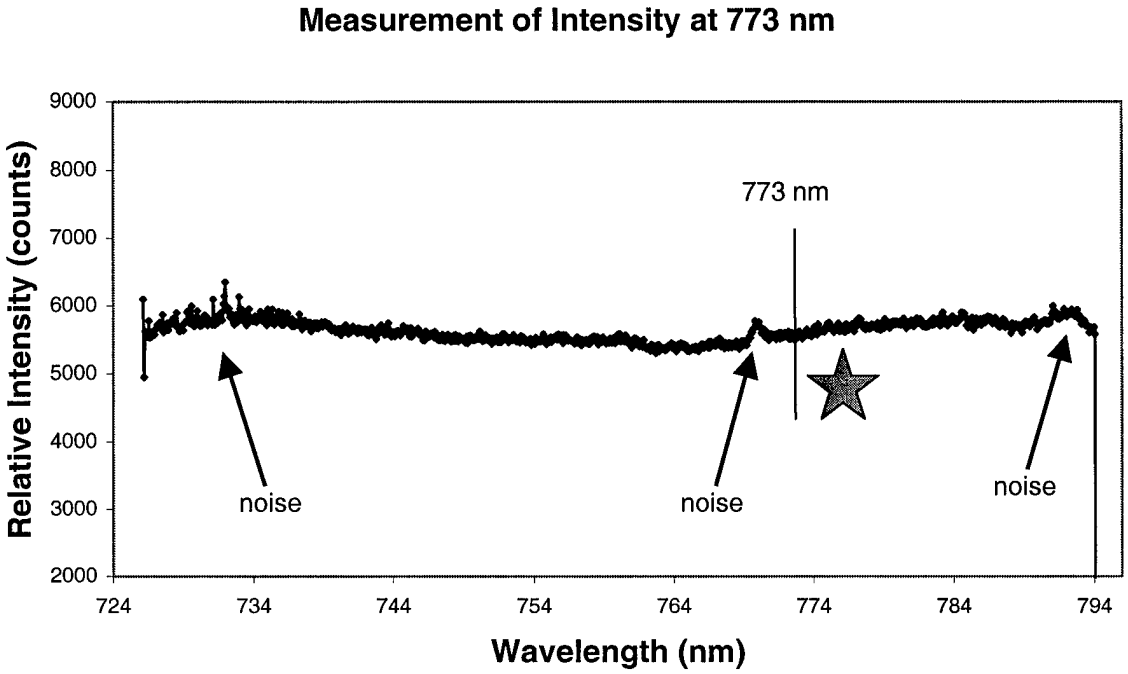

Figure 19. Emission spectrum of a weak intensity at 773 nm. Monochrometer incoming slit width is 200 μm with a period of integration of 6 minutes. Due to the noise inherent to the instrumentation, it is difficult to see the "hump" of intensity. Compare the same position on the chart (star) with that in figure 20. Note that the starred region in figure 20 is more flat.

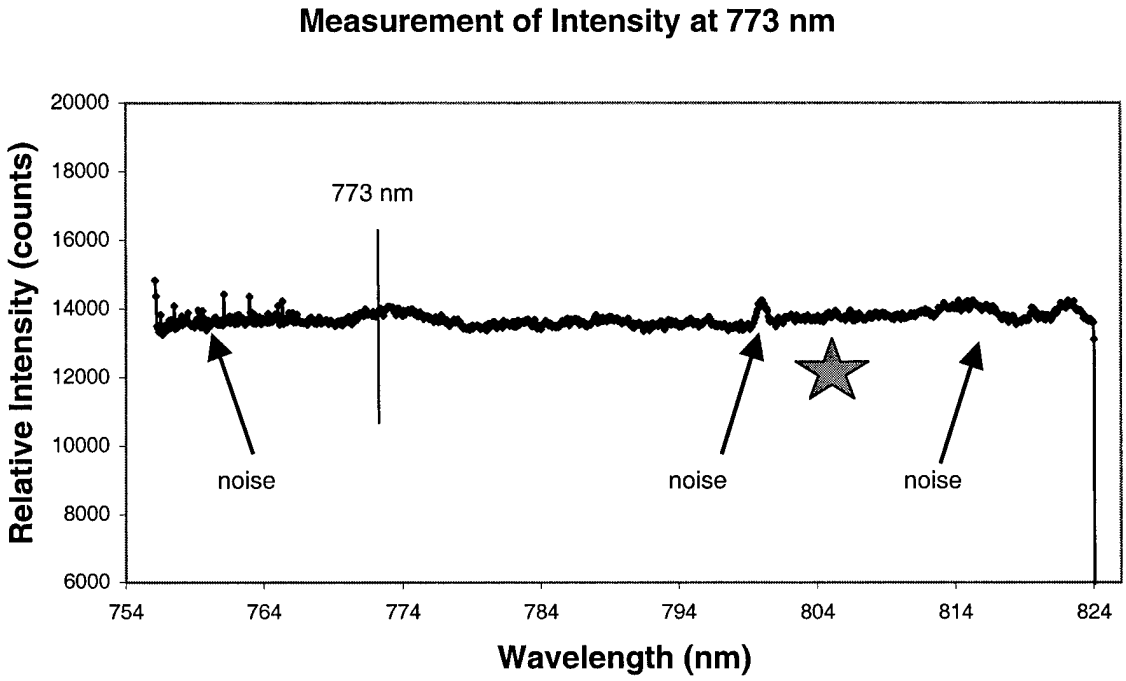

Figure 20. Emission spectrum of a weak intensity at 773 nm (second graph). Monochrometer incoming slit width is 200 μm with a period of integration of 6 minutes. Compare the same position on the chart (star) with that in figure 19. The current position on the chart where 773 nm currently is at is noticeably different from that in figure 19.

The line at 773 nm is the only visibly noticeable intensity to be found in the entire spectrum from 450 nm to 1150 nm. The emissions that are added to this resulting in the reading found in figure 18 must be weak enough to not be recorded individually.

VI. Conclusions and Recommendations

6.1 Overview

This chapter begins by presenting the conclusion drawn from the results of the current research. Next, it offers recommendations based on the findings of the specific topics addressed in this document.

6.2 Conclusions

This research was experimental in nature. The current instrumentation is not sensitive enough to detect the hydroxyl nightglow. It is unknown what created the weak intensity at 773 nm, though it is a major contributor to the emission intensity received of all wavelengths in the visible and near infrared spectrum.

6.3 Recommendations

Equipment that is more sensitive to weak signals should be used. A Fourier transform spectrometer or a Michelson interferometer have both been utilized aboard satellite and space shuttle experiments and have worked with great success. Since no OH was measured, an amplification attachment to the original instrumentation would not be fruitful.

The experiment should yield best results in the early spring or fall. In these cool months, there will be less moisture in the atmosphere. The less moisture there is in a vertical column of atmosphere, the less absorption of the emissions by water vapor. Frost

buildup is an annoying problem to combat. Since the experiment must be performed on cloud-free nights, it would be best to avoid experimentation in the winter months.

Appendix: Photos of Hardware

Figure 21. Picture of the Meade 12" diameter LX-200 Schmidt-Cassegrain telescope (with tripod). All attempts at capturing nightglow radiation were made with the telescope pointing to the zenith. The optic fiber is hanging from the smaller end.

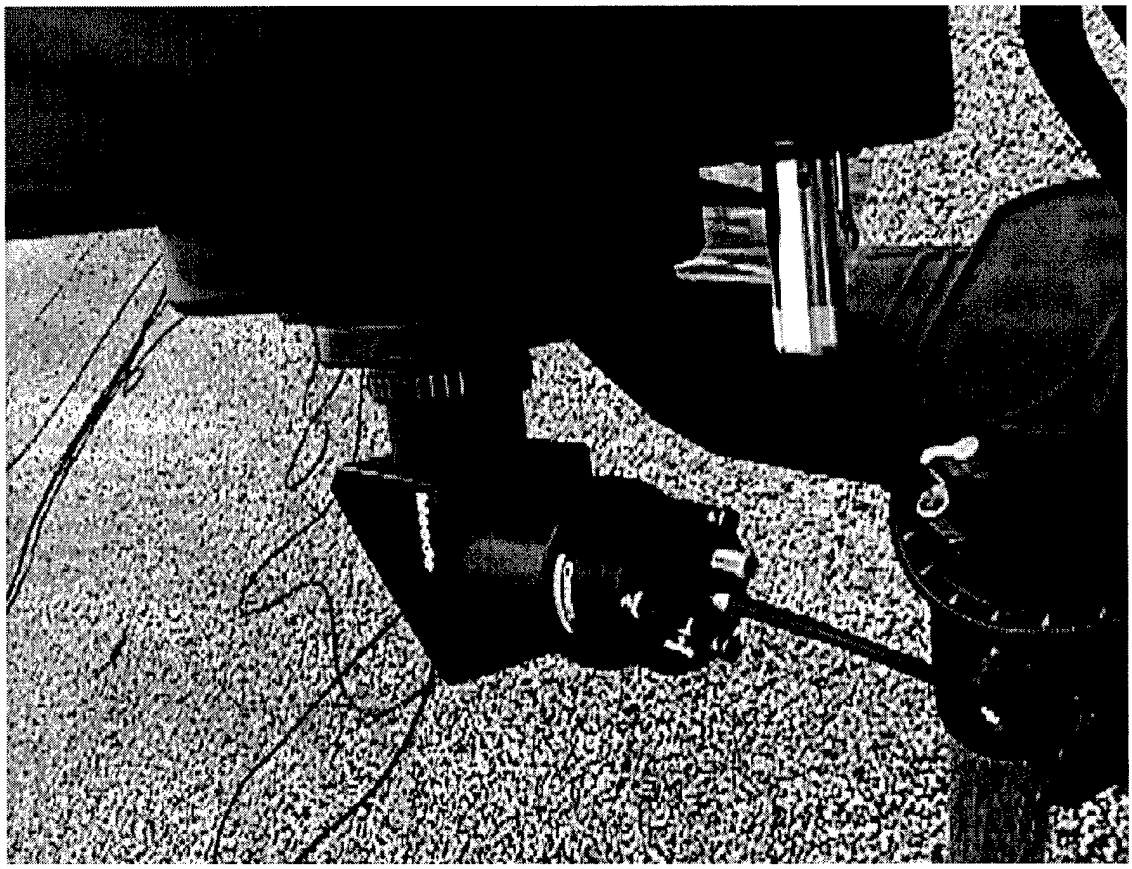

Figure 22. Picture of the telescope and fiber optic coupling. Nightglow is focused through the telescope into the fiber optic cable, which is contained in a cylinder. The cylinder has an additional focusing lens. The telescope's eyepiece was removed.

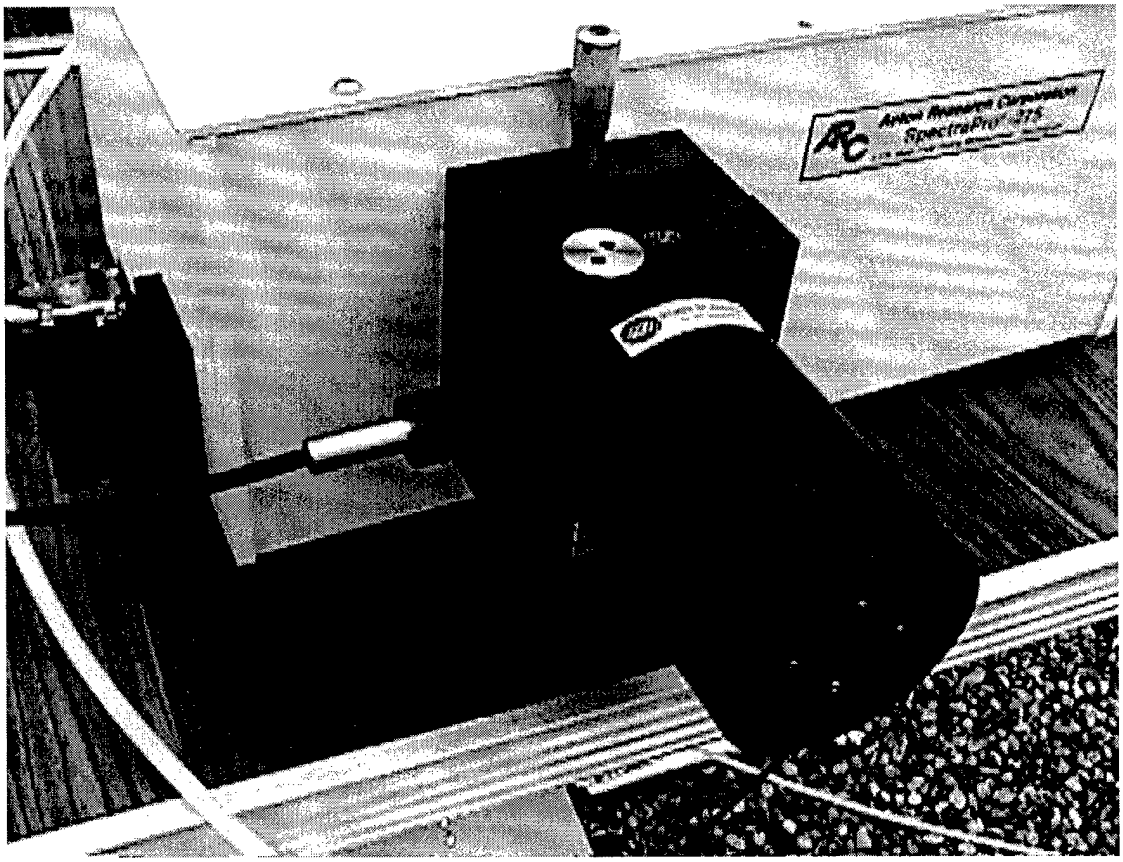

Figure 23. Picture of the fiber optic and ARC Spectrapro 275 monochrometer coupling. Radiation leaves the fiber and enters the monochrometer. The black cylinder shown contains mirrors to help align the radiation to the monochrometer's opening slit.

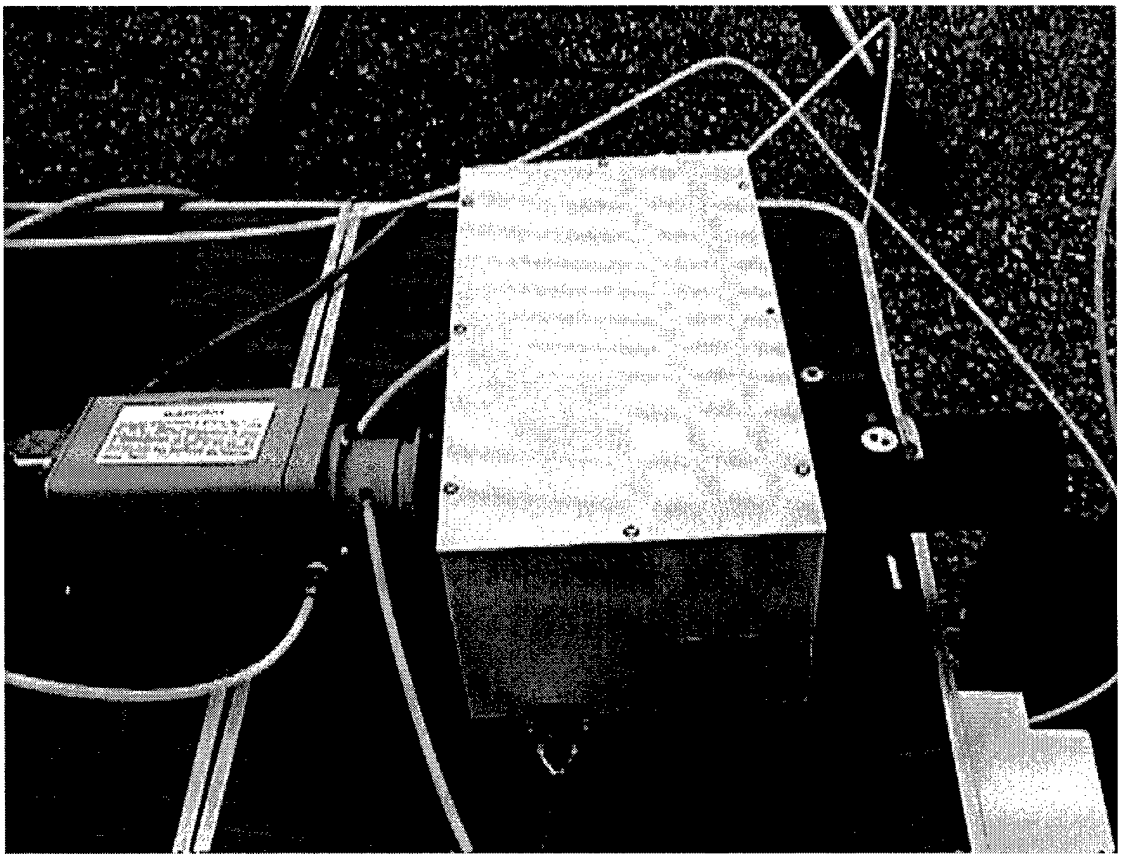

Figure 24. Picture of the detector (left), monochrometer (center), and optic fiber (right). The grating inside the monochrometer spreads the signal into a wavelength orderly spectrum. The desired wavelength interval enters the detector, where the photoelectric diode array within the detector measures intensity.

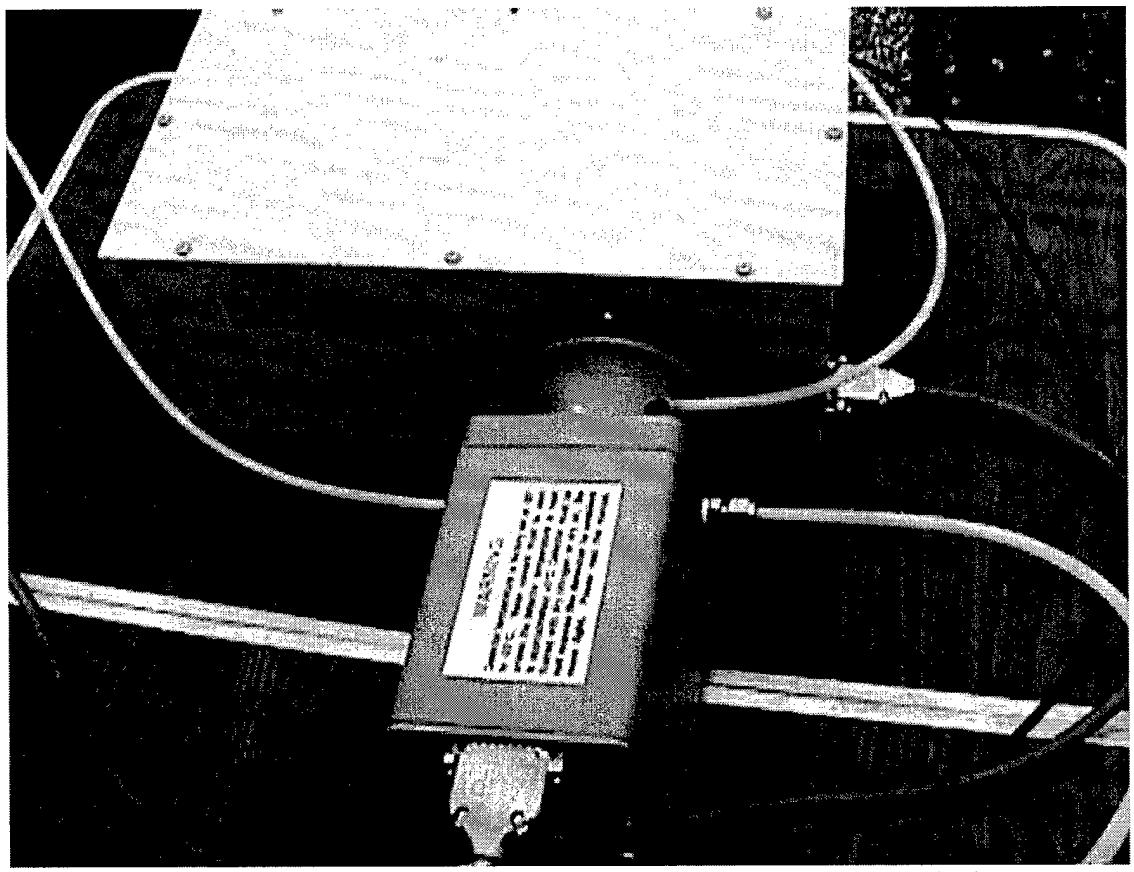

Figure 25. Picture of the Princeton Instruments ST-121 photoelectric diode detector. Note the three white plastic tubes entering the detector (center of picture). One delivers nitrogen gas (to remove moisture) and the other two recirculate water (to cool). Data leaves the detector via the connector (bottom of picture).

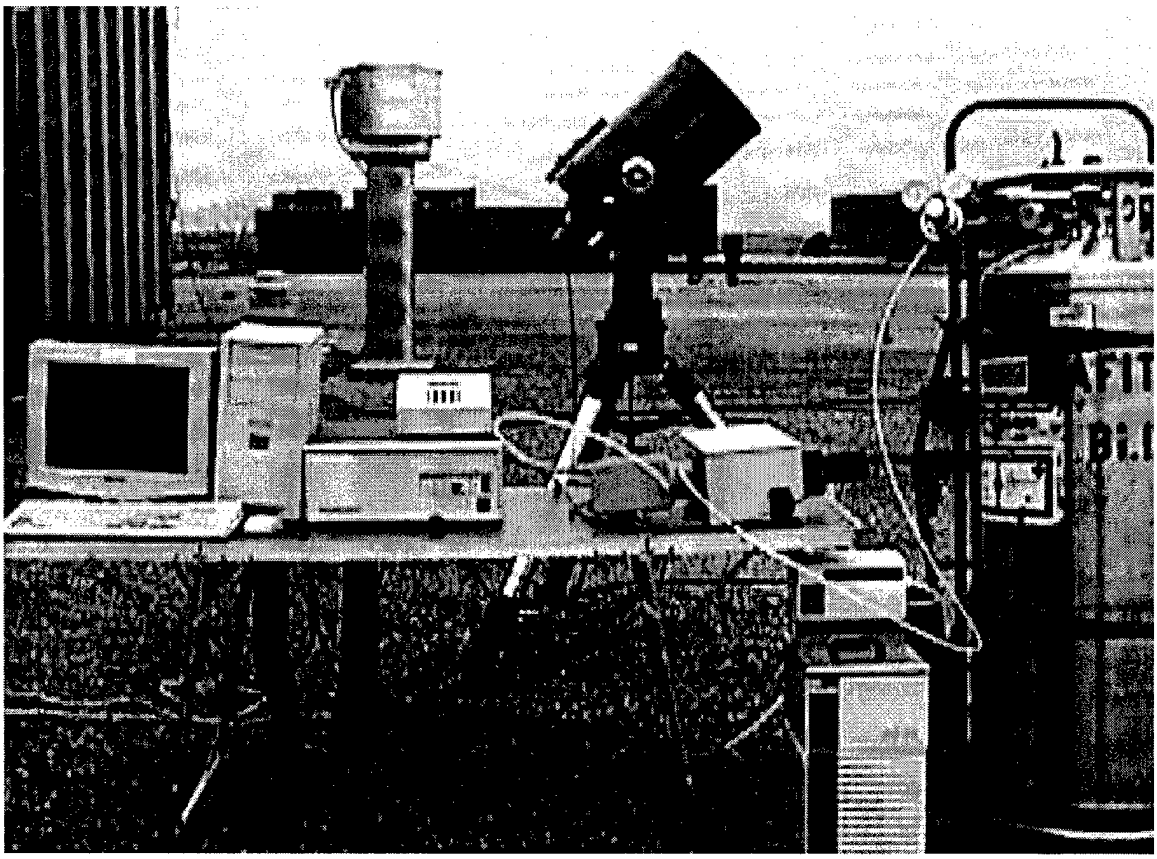

Figure 26. Picture of the field experiment setup (all equipment). Radiation collected by the telescope is sent via the optic fiber into the monochrometer and detector (right edge of table). The detected signal is passed through the controller (large box, center of table) to the computer (left edge of table). The keypad unit on the controller is used to move the grating within the monochrometer to the desired wavelength interval. The nitrogen tank (extreme right) and recirculator (under right edge of table) are also shown.

Bibliography

Abreu, V.J. and J.H. Yee. "Diurnal and Seasonal Variation of the Nighttime OH (8-3) Emission at Low Latitudes," J. Geophys. Res.: 11949-11957 (1989)

Andrews, D.G. Middle Atmosphere Dynamics. New York: Academic Press, 1987.

Bellaire, P.J. Spectral Signature of the Earth's Night Airglow Observed from the Space Shuttle. Ph.D. dissertation. Air Force Institute of Technology (AU), Wright-Patterson AFB OH, July 1997. (ADA327164).

Bernath, P.F. Spectra of Atoms and Molecules. New York: Oxford University Press, 1995

Brown, J.M. Molecular Spectroscopy. New York: Oxford University Press, 1998

Holton, J.R. An Introduction to Dynamic Meteorology. New York: Academic Press, 1992

Hooke, W.H., "Gravity Waves". Mesoscale Meteorology and Forecasting. P.S. Ray, American Meteorological Society: 272-287 (1986)

Lowe, R.P. and D.N. Turnbull. "Comparison of ALOHA-93, ANLC-93, and ALOHA-90 Observations of the Hydroxyl Rotational Temperature and Gravity Wave Activity," Geophys. Res. Lett.: 2813-2816 (1995)

Lowe, R.P., L.M. LeBlanc and K.L. Gilbert. "WINDII/UARS Observation of Twilight Behavior of the Hydroxyl Airglow, at Mid-Latitude Equinox", J. Atmos. & Terr. Phys.: 1863-1869 (1996)

Makhlouf, U., E. Dewan, J.R. Isler and T.F. Tuan. "On the Importance of the Purely Gravitationally Induced Density, Pressure, and Temperature Variations in Gravity Waves: Their Application to Airglow Observations," J. Geophys. Res.: 4103-4111 (1990)

Meinel, A.B. "OH emission bands in the spectrum of the night sky I", Astrophys. J.: 555-564 (1950)

Smith, D.R., W.M. Blumberg, R.M. Nadile, S.J. Lipson, E.R. Huppi, N.B. Wheeler, and J.A. Dodd. "Observation of High-N Hydroxyl Pure Rotation Lines In Atmospheric Emission Spectra by the CIRRIS 1A Space Shuttle Experiment", Geophys. Res. Lett.: 593-596 (1992)

Streit, G.E. and H.S. Johnson. "Reactions and Quenching of Vibrationally Excited Hydroxyl Radicals", J. Chem. Phys.: 95-103 (1976)

Takahashi, H. and P.P. Batista. "Simultaneous Measurements of OH (9,4), (8,3), (7,2), (6,2), and (5,1) Bands in the Airglow", J. Geophys. Res.: 5632-5642 (1981)

Truhlar, D.G. Spectra of Atoms and Molecules. New York: Oxford University Press, 1995

Turnbull, D.N. and R.P. Lowe. "Temporal Variations in the Hydroxyl Nightglow Observed During ALOHA-90," Geophys. Res. Lett.: 1345-1348 (1991)

Turnbull, D.N. and R. P. Lowe. "Vibrational Population Distribution in the Hydroxyl Night Airglow," Can. J. Phys.: 245-250 (1982)

Wallace, J.M. and P.V. Hobbs. Atmospheric Science: An Introductory Survey. New York: Academic Press, 1977

Vita

Captain Erin C.W. Willingham was born in Lincoln, Nebraska in He graduated from Smith High School in Fayetteville, North Carolina in June 1990. He entered undergraduate studies at the University of Nebraska at Lincoln where he graduated with a Bachelor of Science degree in Meteorology in December 1994. He was commissioned through the Detachment 465 AFROTC at the University of Nebraska.

His first assignment was at Kadena AB, Okinawa, Japan as an operational meteorologist in February 1995. In March 1997, he was assigned to 325th Operational Support Squadron, Tyndall AFB as the wing weather officer. In August 1999, he entered the Graduate Meteorology program, School of Engineering and Management, Air Force Institute of Technology. Upon graduation, he will be assigned to the Air Force Weather Agency headquarters at Offutt AFB, Nebraska in May 2001.

Captain Willingham is a member of the American Meteorological Society. He has a wife, and a son,

REPORT DOCUMENTATION PAGE

Form Approved
OMB No. 074-0188

1. REPORT DATE *(DD-MM-YYYY)*	2. REPORT TYPE	3. DATES COVERED *(From – To)*
09-03-2001	Master's Thesis	Aug 1999 – Mar 2001

4. TITLE AND SUBTITLE

INVESTIGATION OF GRAVITY WAVES VIA THE ROTATIONAL TEMPERATURE OF HYDROXYL NIGHTGLOW

5a. CONTRACT NUMBER

5b. GRANT NUMBER

5c. PROGRAM ELEMENT NUMBER

6. AUTHOR(S)

Willingham, Erin C.W., Captain, USAF

5d. PROJECT NUMBER

5e. TASK NUMBER

5f. WORK UNIT NUMBER

7. PERFORMING ORGANIZATION NAMES(S) AND ADDRESS(S)

Air Force Institute of Technology
Graduate School of Engineering and Management (AFIT/EN)
2950 P Street, Building 640
WPAFB OH 45433-7765

8. PERFORMING ORGANIZATION REPORT NUMBER

AFIT/GM/ENP/01M-09

9. SPONSORING/MONITORING AGENCY NAME(S) AND ADDRESS(ES)

AFWA/DNT
Attn: Major Michael Farrar
106 Peacekeeper Dr., Ste. 2N3
Offutt AFB, NE 62225-5026 DSN: 271-4562

10. SPONSOR/MONITOR'S ACRONYM(S)

11. SPONSOR/MONITOR'S REPORT NUMBER(S)

12. DISTRIBUTION/AVAILABILITY STATEMENT

APPROVED FOR PUBLIC RELEASE; DISTRIBUTION UNLIMITED.

13. SUPPLEMENTARY NOTES

14. ABSTRACT

Measurement of the vibration and rotation bands of mesospheric hydroxyl radicals (OH) has been conducted during the past two decades using ground-based and space-based interferometers to take temperature and wind measurements from 70-100 km in altitude. Gravity waves that pass through the mesosphere can be measured by determining the variance over time of the rotational temperature of the OH emissions. Several attempts were made to take spectrum measurements of the nightglow from hydroxyl radicals in the mesosphere using a custom hardware configuration that included a telescope and grating monochrometer optimized for the visible and near infrared. Quantifying gravity wave activity was the ultimate objective of this experiment. No spectrum of OH nightglow was recorded. The instrumentation was not sensitive enough to pick up the weak signal. This thesis is primarily a characterization of the equipment, its capabilities, and its limitations.

15. SUBJECT TERMS

hydroxyl, nightglow, airglow, gravity waves, rotational temperature.

16. SECURITY CLASSIFICATION OF:			17. LIMITATION OF ABSTRACT	18. NUMBER OF PAGES	19a. NAME OF RESPONSIBLE PERSON
a. REPORT	b. ABSTRACT	c. THIS PAGE			Lt. Col. Glen P. Perram, ENP
U	U	U	UU	66	19b. TELEPHONE NUMBER *(Include area code)* (937) 255-3636, ext 4504 DSN:785-3636, ext 4504

Standard Form 298 (Rev. 8-98)
Prescribed by ANSI Std. Z39-18

Form Approved
OMB No. 074-0188